Nutritional modulation of heart failure in mitochondrial pyruvate carrier–deficient mice

Kyle S. McCommis [1,2] ✉, Attila Kovacs[1], Carla J. Weinheimer[1], Trevor M. Shew[1], Timothy R. Koves[3], Olga R. Ilkayeva [3], Dakota R. Kamm[2], Kelly D. Pyles[2], M. Todd King[4], Richard L. Veech[4], Brian J. DeBosch [5], Deborah M. Muoio [3], Richard W. Gross [1,6] and Brian N. Finck[1]

The myocardium is metabolically flexible; however, impaired flexibility is associated with cardiac dysfunction in conditions including diabetes and heart failure. The mitochondrial pyruvate carrier (MPC) complex, composed of MPC1 and MPC2, is required for pyruvate import into the mitochondria. Here we show that MPC1 and MPC2 expression is downregulated in failing human and mouse hearts. Mice with cardiac-specific deletion of *Mpc2* (CS-MPC2$^{-/-}$) exhibited normal cardiac size and function at 6 weeks old, but progressively developed cardiac dilation and contractile dysfunction, which was completely reversed by a high-fat, low-carbohydrate ketogenic diet. Diets with higher fat content, but enough carbohydrate to limit ketosis, also improved heart failure, while direct ketone body provisioning provided only minor improvements in cardiac remodelling in CS-MPC2$^{-/-}$ mice. An acute fast also improved cardiac remodelling. Together, our results reveal a critical role for mitochondrial pyruvate use in cardiac function, and highlight the potential of dietary interventions to enhance cardiac fat metabolism to prevent or reverse cardiac dysfunction and remodelling in the setting of MPC deficiency.

The myocardium requires vast amounts of chemical energy stored in nutrients to fuel cardiac contraction. To maintain this high metabolic capacity, the heart is extremely flexible and can adapt to altered metabolic fuel supplies during diverse developmental, nutritional or physiologic conditions. Cardiac mitochondria are capable of oxidizing fatty acids, pyruvate (derived from either glucose or lactate), ketone bodies or amino acids when needed. Whereas fatty acids are considered a predominant fuel source for normal adult hearts[1,2], several physiological conditions can increase the importance of other substrates for cardiac metabolism. For example, the mammalian foetal heart relies mostly on anaerobic glycolysis until oxygen is abundant and the oxidative capacity of the heart matures ~15–20 d postnatally in rodents[3–5]. In the adult heart, myocardial lactate[6] and ketone body[7–9] extraction and oxidation can be greatly enhanced depending on the physiological conditions.

A hallmark of heart failure in mice and humans is a metabolic switch away from mitochondrial oxidative metabolism[10–13]. Fatty acid oxidation (FAO) is reduced in the failing heart as a result of deactivating the expression of a wide transcriptional program for FAO enzymes and transporters[10,14–16] and other mitochondrial metabolic enzymes[10,12,13]. The deactivation of mitochondrial metabolism in pathological heart remodelling leads to an increased reliance on glycolysis[17], but decreased glucose/pyruvate oxidation[18] results in a mismatch that may cause energetic defects, altered redox status or accumulation of metabolic intermediates with signalling and physiological effects.

Many aspects of cardiac pyruvate/lactate metabolism remain to be fully understood. For pyruvate to enter the mitochondrial matrix and be oxidized, it must be transported across the inner mitochondrial membrane by the mitochondrial pyruvate carrier (MPC), a hetero-oligomer composed of MPC1 and MPC2 proteins[19,20]. Pyruvate oxidation occurs in the mitochondrial pyruvate dehydrogenase (PDH) complex and previous studies have shown that impaired cardiac PDH activity in mouse heart limits metabolic flexibility[21–24]. However, PDH deactivation does not cause overt cardiac remodelling or dysfunction in the absence of further cardiac stress[21–24]. Another metabolic fate for pyruvate is carboxylation, which is an anaplerotic reaction capable of replenishing tricarboxylic acid (TCA) cycle intermediates. In cardiac myocytes, pyruvate carboxylation can occur in the cytosol via malic enzyme 1, or in the mitochondrial matrix via malic enzymes 2 or 3, or pyruvate carboxylase. Because MPC deletion could affect both pyruvate carboxylation and oxidation, we hypothesized that impaired MPC activity would have a greater impact on pyruvate metabolism and regulation of cardiac metabolic flexibility compared to modulating PDH activity alone.

In the present study, we demonstrate that MPC expression is decreased in failing human and mouse hearts, and that genetic deletion of the MPC in mice leads to cardiac remodelling and dysfunction. This heart failure can be prevented or even reversed by providing a high-fat (HF), low-carbohydrate 'ketogenic' diet. A 24 h fast in mice also provided significant improvement in heart remodelling. Diets with higher fat content, but enough carbohydrates to limit ketosis also significantly improved heart failure in mice lacking cardiac MPC expression. Gene expression, metabolomic analyses and cardiac respiration analyses all suggest improved myocardial fat metabolism, rather than increased ketone body metabolism, as the mechanism driving these improvements in heart failure. These results demonstrate that MPC deficiency induces cardiac

[1]Department of Medicine, Washington University School of Medicine, St. Louis, MO, USA. [2]Department of Biochemistry & Molecular Biology, Saint Louis University School of Medicine, St. Louis, MO, USA. [3]Duke Molecular Physiology Institute, Duke University School of Medicine, Durham, NC, USA. [4]Laboratory of Metabolic Control, National Institute on Alcohol Abuse and Alcoholism, National Institute of Health, Bethesda, MD, USA. [5]Departments of Pediatrics and Cell Biology & Physiology, Washington University School of Medicine, St. Louis, MO, USA. [6]Department of Chemistry, Washington University, St. Louis, MO, USA. ✉e-mail: kyle.mccommis@health.slu.edu

dysfunction in mice, and that dietary manipulations can prevent or reverse cardiomyopathy in this model.

Results

MPC is downregulated in human and mouse heart failure. We first examined the expression of MPC proteins in heart samples of human patients obtained at the time of left-ventricular assist device (LVAD) implantation or cardiac transplantation. We compared these samples to cardiac donor tissue from hearts that were nonfailing but deemed unsuitable for transplant. As expected, quantitative PCR with reverse transcription (RT–qPCR) analyses indicated that failing human hearts exhibited increased expression of natriuretic peptides and fibrotic collagens compared to nonfailing controls (Extended Data Fig. 1a) as well as decreased expression of *PPARGC1A*, *PPARA* and mitochondrial FAO enzymes (Extended Data Fig. 1b). Failing hearts also expressed lower levels of *MPC1* and *MPC2* compared to nonfailing controls at both the messenger RNA and protein level (Fig. 1a–c). Other mitochondrial proteins such as VDAC1 and the complex I subunit NDUFB8 and complex II subunit SDHB were also reduced in the failing hearts (Fig. 1c), further supporting the notion that heart failure is associated with a general loss of mitochondrial abundance and oxidative function[10–16]. However, the complex III subunit UQCRC2 and complex 5 subunit ATP5A were not downregulated in the failing hearts (Fig. 1c), and thus the MPC proteins trended to be, or were significantly, reduced depending on how expression is normalized to other mitochondrial or cytosolic proteins (Extended Data Fig. 1c,d). Failing hearts showed improvements in metabolic gene expression after LVAD placement, but natriuretic peptides and collagens were not significantly improved (Fig. 1a,b and Extended Data Fig. 1a,b). *Mpc1* and *Mpc2* were also lower in wild-type (WT) mouse hearts subjected to the heart failure model of transverse aortic constriction and myocardial infarction (TAC + MI) than to the sham treatment (Extended Data Fig. 1e). Thus, consistent with recent data[25], human heart failure is associated with decreased cardiac MPC expression. While this reduced expression could be due to the general downregulation of mitochondrial oxidative pathways, we suspect that MPC loss might contribute to the reduced glucose/pyruvate oxidation that occurs in heart failure despite elevated rates of glycolysis[17,18].

CS-MPC2−/− mice display altered pyruvate metabolism and TCA cycle defects. To determine whether this decrease in cardiac MPC expression was an adaptive process in heart failure or contributes to the cardiac remodelling and dysfunction, we generated cardiac-specific *Mpc2* knockouts (CS-MPC2−/−) using our established *Mpc2* floxed mouse[26–28] and mice expressing Cre under the endogenous myosin light chain 2v promoter[29]. CS-MPC2−/− mice had complete loss of cardiac *Mpc2* gene expression (Extended Data Fig. 1f). Loss of MPC2 led to destabilization of MPC1 protein as well, and neither MPC2 nor MPC1 protein was detected in CS-MPC2−/− mouse hearts (Fig. 1d). CS-MPC2−/− heart mitochondria displayed drastically reduced pyruvate-stimulated oxygen consumption rates (OCRs), and were resistant to inhibitory effects

of the MPC inhibitor UK-5099 on respiration (Fig. 1e). *Mpc2* flox heterozygotes expressing Cre (CS-MPC2+/− mice) displayed a ~50% decrease in MPC expression and pyruvate-stimulated respiration (Fig. 1d–e and Extended Data Fig. 1f). Isolated mitochondria from CS-MPC2+/− and CS-MPC2−/− hearts displayed normal OCR on palmitoyl carnitine/malate, glutamate/malate and succinate (Fig. 1f), suggesting a specific defect in mitochondrial pyruvate metabolism. CS-MPC2−/− mice also displayed slight, but significantly elevated blood lactate levels (Extended Data Fig. 1g), consistent with the heart as an appreciable lactate-consuming organ or indicating that the CS-MPC2−/− hearts were producing lactate.

To more thoroughly investigate how loss of MPC expression altered mitochondrial metabolism, targeted metabolomics analyses were conducted on hearts from 6-week-old female mice (Fig. 1g,h and Supplementary Table 1). CS-MPC2−/− hearts contained decreased acetyl-CoA levels, and an accumulation of TCA cycle intermediates upstream of acetyl-CoA (fumarate, malate and oxaloacetate (aspartate measured as surrogate)) (Fig. 1g,h and Supplementary Table 1). Pyruvate accumulated, but myocardial lactate concentrations were unaltered, leading to a decreased lactate to pyruvate ratio in the CS-MPC2−/− hearts (Fig. 1g,h and Supplementary Table 1). The elevated blood lactate (Extended Data Fig. 1g) and unchanged myocardial lactate concentrations potentially suggest elevated lactate release from the CS-MPC2−/− hearts, or that these hearts were not efficiently using lactate from the blood. These results are similar to lactate and pyruvate concentrations of perfused rat hearts treated with the MPC inhibitor α-cyanocinnimate[30]. Transamination to alanine is another potential fate of pyruvate, and CS-MPC2−/− hearts displayed significantly elevated alanine concentrations (Fig. 1g,h and Supplementary Table 1). The decreased lactate/pyruvate ratio suggests a decreased cytosolic NADH/NAD+ redox ratio. However, analysis of other mitochondrial redox-linked reactions does not provide a consistent conclusion on redox status as the αketoglutarate/succinyl-CoA ratio was increased, and the succinate/fumarate ratio was decreased in CS-MPC2−/− hearts (Supplementary Table 1). Altogether, these findings indicated that loss of cardiac MPC results in defective mitochondrial pyruvate metabolism, alterations in TCA cycle flux and potentially dysregulated redox status.
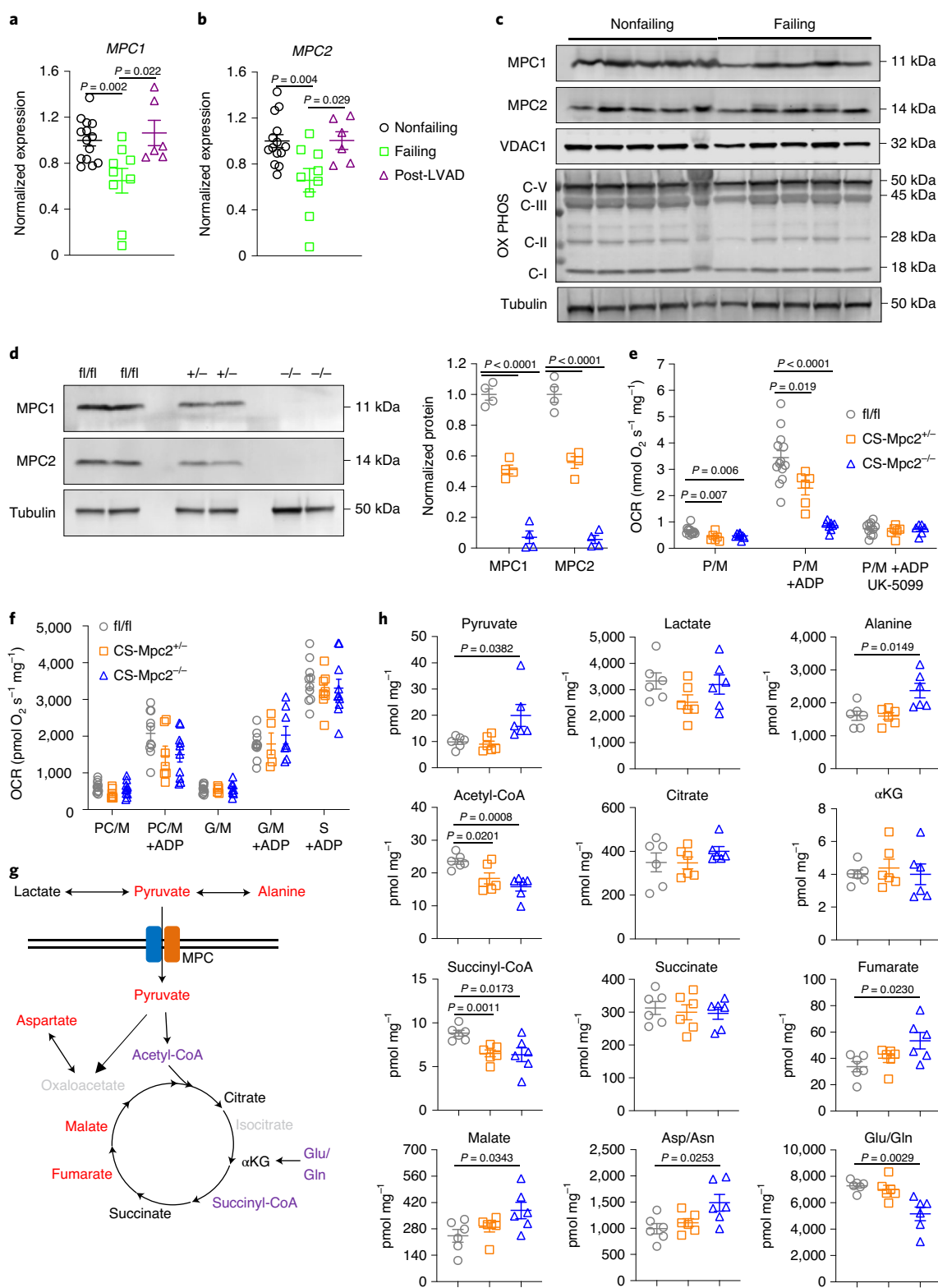
CS-MPC2−/− mice develop dilated cardiomyopathy. Hearts from 6-week-old CS-MPC2−/− mice appeared normal by echocardiography, but heart weight and hypertrophic gene expression were slightly elevated in these young mice (Fig. 2a–c and Extended Data Figs. 1h–j and 2a–h). Cardiac enlargement and decreased contractile function was well-evident at 10 weeks and further worsened at 16 weeks of age (Fig. 2a–d and Extended Data Fig. 2a–h). Increased ventricular mass was confirmed at death (Fig. 2e,f), as was increased lung weight indicative of lung oedema (Fig. 2g). CS-MPC2−/− hearts also showed dramatically altered gene expression markers of heart failure and fibrosis (Fig. 2h,i). CS-MPC2+/− heterozygotes displayed normal cardiac size, function and hypertrophic gene expression (Fig. 2a–i and Extended Data Fig. 2a–h), suggesting that MPC haploinsufficiency or Cre expression alone was not provoking this

Fig. 1 | MPCs are downregulated in human heart failure, and deletion of cardiac MPC2 results in TCA cycle dysfunction. a,b, Gene expression measured by RT–qPCR for *MPC1* (**a**) and *MPC2* (**b**) normalized to *RPLP0* from human hearts of nonfailing, failing and failing hearts post-LVAD implant (*n* = 14, 9 and 6 for nonfailing, failing and post-LVAD, respectively). **c**, Western blot images for MPC1, MPC2, VDAC1, OX PHOS subunits and α-tubulin in nonfailing and failing human heart tissue (*n* = 5). **d**, Representative western blots of MPC1, MPC2 and α-tubulin of mouse heart tissue and densitometry quantification (*n* = 4). **e**, OCR stimulated by pyruvate/malate (P/M) of isolated cardiac mitochondria before and after addition of ADP and 5 μM of the MPC inhibitor UK-5099 (*n* = 13, 6 and 8 for fl/fl, CS-Mpc2+/− and CS-Mpc2−/−, respectively). **f**, OCRs stimulated by palmitoyl carnitine/malate (PC/M), glutamate/malate (G/M) or succinate (S) before or after the addition of ADP measured from isolated cardiac mitochondria (*n* = 10, 8 and 10 for fl/fl, CS-Mpc2+/− and CS-Mpc2−/−, respectively). **g**, Schematic of TCA cycle alterations measured by metabolomic analyses of heart tissue. Red, increased; purple, decreased; black, unchanged (comparing fl/fl to CS-Mpc2−/−) and grey, unmeasured. **h**, TCA cycle intermediates (pyruvate, lactate, alanine, acetyl-CoA, citrate, α-ketoglutarate, succinyl-CoA, succinate, fumarate, malate, aspartate/asparagine and glutamate/glutamine) measured by mass spectrometry from 6-week-old heart tissue (*n* = 6). Mean ± s.e.m. shown within dot plots. Each symbol represents an individual sample. Two-tailed unpaired Student's *t*-test.

heart failure phenotype. WT C57BL6/J mice treated with the MPC inhibitor MSDC-0602, currently in development to treat diabetes and nonalcoholic steatohepatitis[28], also did not show cardiac enlargement or cardiac hypertrophic gene expression (Extended Data Fig. 2i,j), although a beneficial pharmacologic effect on fatty liver disease was observed in these mice[28]. Together, these results indicate that complete loss of MPC expression, but not partial loss

or pharmacologic MPC inhibition, results in cardiac remodelling and dysfunction.

Other than *Cpt1b*, this group of CS-MPC2⁻/⁻ hearts did not show major downregulation of FAO enzymes and transporters associated with FAO as is typical for failing hearts (Fig. 2j and Extended Data Fig. 2k). However, many other PPARα target genes were downregulated in these failing hearts (Extended Data Fig. 2l). CS-MPC2⁻/⁻
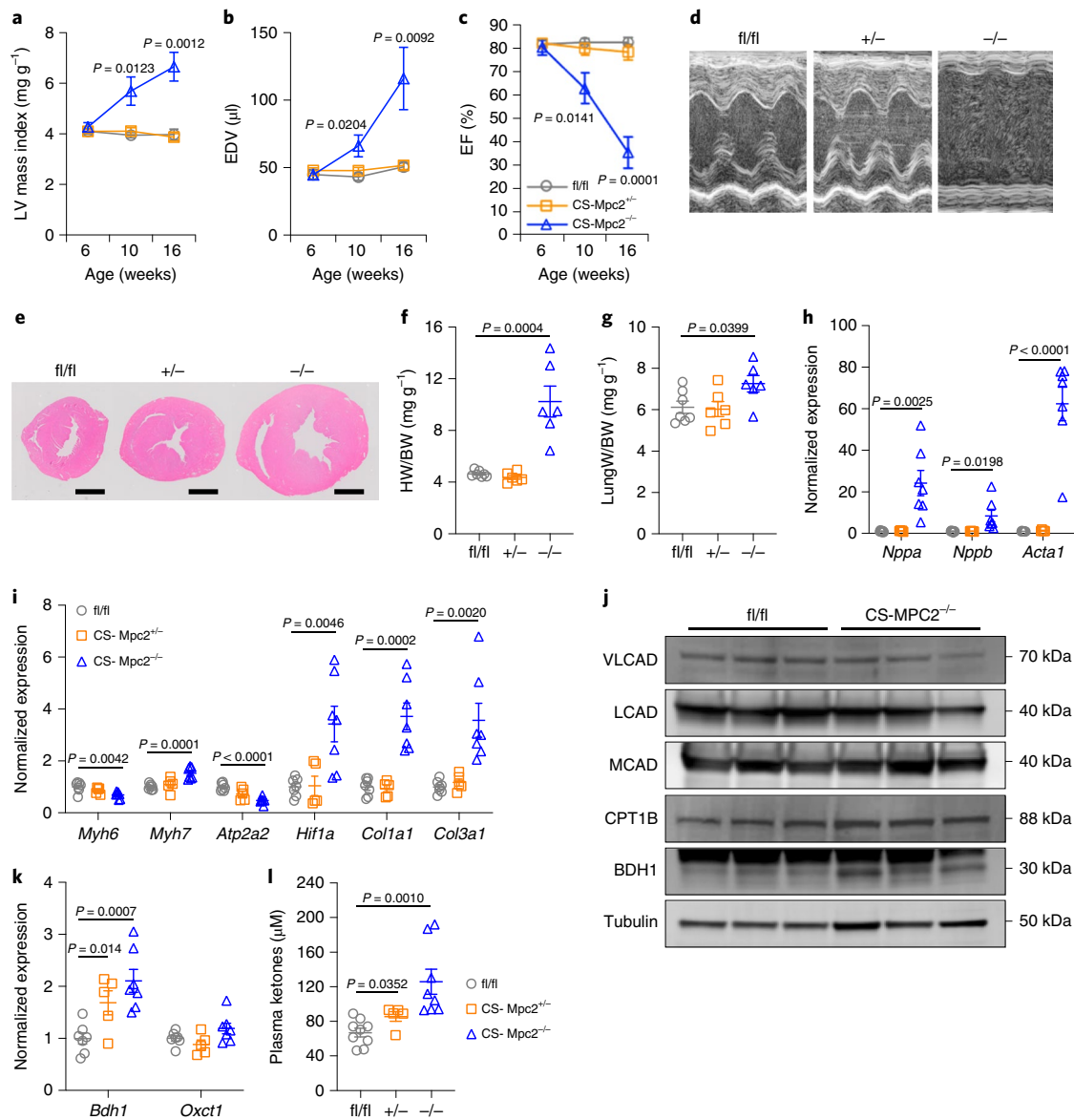
Fig. 2 | CS-MPC2^−/−^ mice develop dilated cardiomyopathy. a–c, Echocardiography measures of LV mass index (**a**), end-diastolic volume (EDV) (**b**) and ejection fraction (EF) (**c**) of mice at 6, 10 and 16 weeks of age (n = 7, 10 and 9 for fl/fl, CS-Mpc2^+/−^ and CS-Mpc2^−/−^, respectively). **d**, Representative M-mode electrocardiogram images of 16-week-old mice. **e**, Representative short-axis heart images stained by H&E (scale bar, 1 mm). For **d** and **e**, experiments were repeated four times with small independent groups of littermate mice, with similar results obtained. **f,g**, Heart weight (HW) (**f**) and lung weight (**g**) normalized to body weight (BW) from 16-week-old mice (n = 7, 6 and 6 for fl/fl, CS-Mpc2^+/−^ and CS-Mpc2^−/−^, respectively). **h,i**, Gene expression markers of cardiac hypertrophy/failure (*Nppa*, *Nppb* and *Acta1* (**h**), and *Myh6*, *Myh7*, *Atp2a2*, *Hif1a*, *Col1a1* and *Col3a1* (**i**)) from 16-week-old mouse hearts (n = 7, 5 and 7 for fl/fl, CS-Mpc2^+/−^ and CS-Mpc2^−/−^, respectively). **j**, Western blot images of VLCAD, LCAD, MCAD, CPT1B, BDH1 and α-tubulin from whole cardiac lysates (n = 3). **k**, Gene expression for *Bdh1* and *Oxct1* from 16-week-old mouse hearts (n = 7, 5 and 7 for fl/fl, CS-Mpc2^+/−^ and CS-Mpc2^−/−^, respectively). **l**, Plasma total ketone body levels from 16-week-old mice (n = 9, 5 and 8 for fl/fl, CS-Mpc2^+/−^ and CS-Mpc2^−/−^, respectively). Mean ± s.e.m. shown within dot plots. Each symbol represents an individual sample. Two-tailed unpaired Student's *t*-test.

hearts exhibited increased expression of BDH1 at the gene and protein level (Fig. 2j,k) and significantly elevated plasma ketone bodies were found in CS-MPC2^−/−^ mice (Fig. 2l). Together, this elevated ketosis and increased BDH1 expression suggests increased ketone body metabolism in the failing CS-MPC2^−/−^ hearts[31,32], which was recently shown to be an adaptive and protective process in heart failure[33].

HF, low-carbohydrate ketogenic diet prevents heart failure in CS-MPC2^−/−^ mice. We hypothesized that the cardiac remodelling and dysfunction in CS-MPC2^−/−^ mice could be improved

by providing nutrients in the diet that could be better used by CS-MPC2^−/−^ hearts. To test this, fl/fl and CS-MPC2^−/−^ mice were fed a low-carbohydrate (1.8%kcal), HF (93.9%kcal) ketogenic diet (KD) or a low-fat (LF) control diet from 6 weeks until 17 weeks of age. KD resulted in the expected increase in ketosis (Fig. 3a and Supplementary Table 2), as well as limited weight gain, decreased blood glucose and decreased plasma insulin concentrations in both fl/fl and CS-MPC2^−/−^ mice (Extended Data Fig. 3a–c, Supplementary Table 2). LF-fed CS-MPC2^−/−^ mice displayed extreme cardiac enlargement and dysfunction on echocardiography (Fig. 3b–d and Extended Data Fig. 3d–n), which was even worse

than that in chow-fed CS-MPC2$^{-/-}$ mice (Fig. 2), potentially due to the increased content of refined sucrose in the LF diet. KD-fed CS-MPC2$^{-/-}$ mice displayed virtually normal cardiac size and function during echocardiography studies at 10 and 16 weeks of age (Fig. 3b–d, Extended Data Fig. 3d–n and Supplementary Video 1). The severe cardiac dysfunction in LF-fed CS-MPC2$^{-/-}$ mice was associated with loss of body weight by 17 weeks of age (Extended Data Fig. 3a), which was driven by loss of adipose tissue fat mass (Extended Data Fig. 3o–s). Nearly 35% of LF-fed CS-MPC2$^{-/-}$ mice died before 17 weeks of age, but all CS-MPC2$^{-/-}$ mice fed KD survived (Fig. 3e). Extreme cardiac enlargement, increased lung oedema and increased cardiomyocyte cross-sectional area (CSA) were observed in LF-fed CS-MPC2$^{-/-}$ mice, but these responses were all completely prevented by feeding KD (Fig. 3f–i). Gene expression markers for heart failure and fibrosis, as well as trichrome fibrosis staining, were all elevated in LF-fed, and completely corrected in KD-fed, CS-MPC2$^{-/-}$ hearts (Fig. 3f,j–n). LF-fed CS-MPC2$^{-/-}$ hearts also displayed altered hypertrophic growth signalling by increased ERK phosphorylation, decreased 5′-AMP-activated protein kinase alpha (AMPKα) phosphorylation, increased mTOR phosphorylation and increased S6-ribosomal protein phosphorylation (Fig. 3o), consistent with increased protein synthesis required to drive pathologic cardiac hypertrophy[34]. Feeding CS-MPC2$^{-/-}$ mice KD completely prevented this aberrant hypertrophic growth signalling (Fig. 3o). Altogether, these results show that KD is able to completely prevent cardiac remodelling and dysfunction of CS-MPC2$^{-/-}$ mice.

KD downregulates cardiac ketone body oxidation and enhances fat metabolism. The chow-fed CS-MPC2$^{-/-}$ mice showed elevated ketone bodies and increased BDH1 expression (Fig. 2j–l), consistent with recent work suggesting an increase in ketone body oxidation in failing hearts[31,32]. LF-fed CS-MPC2$^{-/-}$ mice also displayed an increase in plasma ketone bodies (Fig. 3a), and the failing hearts from these mice showed an upregulation of the ketolytic-enzyme-encoding genes *Bdh1* and *Oxct1*, as well as increases in C4-OH-carnitine and 3-hydroxybutyrate-CoA (Fig. 4a–f). Hearts from both fl/fl and CS-MPC2$^{-/-}$ mice show decreased *Bdh1* and *Oxct1* expression after KD feeding (Fig. 4b–d), in agreement with a previous report demonstrating that the myocardium downregulates ketone body oxidation during KD[35]. Along these lines, the levels of succinyl-CoA, succinate and succinate/succinyl-CoA ratio all suggest increased ketolytic flux in failing LF-fed CS-MPC2$^{-/-}$ hearts that is reduced by KD feeding (Fig. 4g–i and Supplementary Table 3). KD feeding also normalized the levels of free CoA-SH, malonyl-CoA, as well as the expression of malonyl-CoA-generating enzymes *Acaca* and *Acacb* in CS-MPC2 hearts (Fig. 4j–n and Supplementary Table 3). Altogether, these results suggest that the improvements in cardiac remodelling and function from KD feeding were not related to enhanced ketone metabolism.

The failing LF-fed CS-MPC2$^{-/-}$ hearts displayed an accumulation of acylcarnitines and depletion of free carnitine, which was normalized by KD feeding (Fig. 5a–d and Supplementary Table 3). Accumulation of acylcarnitines suggests a decrease in their transport into the mitochondrial matrix and oxidation, as has been shown previously in ischaemia and heart failure[36,37]. Indeed, failing LF-fed CS-MPC2$^{-/-}$ hearts displayed decreased expression of *Ppargc1a*, *Ppara* and many of their target genes for fatty acid transport and metabolism (Fig. 5e–l). KD feeding rescued or strongly elevated the expression of *Ppargc1a*, *Ppara* and its gene targets related to FAO in both fl/fl and CS-MPC2$^{-/-}$ hearts (Fig. 5e–l). The *Ppara* target gene *Hmgcs2*, whose product generates ketone bodies and is normally expressed almost exclusively in the liver, was strongly induced in KD-fed fl/fl and CS-MPC2$^{-/-}$ hearts (Fig. 5l). Cumulatively, these results suggest that KD feeding does not enhance cardiac ketone body metabolism, but rather stimulates FAO, which may be responsible for the improved cardiac remodelling and performance.

Exogenous ketone bodies moderately attenuate cardiac remodelling in CS-MPC2$^{-/-}$ mice. We also wanted to assess whether increased ketosis without altering dietary fat intake was able to improve cardiac function. To test this, CS-MPC2$^{-/-}$ mice were maintained on chow diet and injected intraperitoneally (i.p.) with saline vehicle or 10 mmol kg^{-1} β-hydroxybutyrate (βHB) daily for 2 weeks (Extended Data Fig. 4a). Over this timeframe, vehicle treated CS-MPC2$^{-/-}$ mice displayed worsened left-ventricular (LV) dilation and contractile function, which were either limited or slightly improved by daily βHB administration (Extended Data Fig. 4b–h). At euthanasia, 4 h after the last βHB injection, plasma ketone concentrations were significantly elevated (Extended Data Fig. 4i), but not nearly to the same degree as that under KD feeding (Fig. 3a). Heart weight (Extended Data Fig. 4j) and hypertrophic/fibrotic gene expression (Extended Data Fig. 4k) were only modestly improved by administration of ketone bodies daily on top of carbohydrate-rich chow diet.

In a second attempt to raise ketosis without altering dietary fat, we fed mice a diet supplemented with 16.5%kcal D-β-hydroxybutyrate-(R)-1,3 butanediol monoester 'ketone ester'. For this experiment, mice were fed control or ketone ester diet from 9–15 weeks of age. Ketone ester diet slightly raised plasma ketone bodies (Extended Data Fig. 5a), but did not improve cardiac size or contractile function measured by echocardiography (Extended Data Fig. 5b–e) or heart weight at death (Extended Data Fig. 5f). Last, cardiac gene expression of markers of heart failure were only modestly improved by a ketone ester diet (Extended Data Fig. 5g–i). Thus, two different ways to enhance ketosis without altering dietary fat intake did not drastically improve cardiac size or function in CS-MPC2$^{-/-}$ mice. These results suggest that provision of ketones per se is not sufficient to improve heart failure in KD-fed CS-MPC2$^{-/-}$ mice.

HF diets significantly improve heart failure in CS-MPC2$^{-/-}$ mice. To dissect the importance of dietary fat and myocardial FAO, we

Fig. 3 | KD can prevent heart failure in CS-MPC2$^{-/-}$ mice. a, Plasma total ketone bodies from LF- or KD-fed mice ($n = 8$, 5, 9 and 7 for fl/fl LF, CS-Mpc2$^{-/-}$ LF, fl/fl KD and CS-Mpc2$^{-/-}$ KD, respectively). **b–d**, Echocardiography measures of LV mass index (**b**), end-diastolic volume (EDV) (**c**) and ejection fraction (EF) (**d**) of LF- or KD-fed mice at 16 weeks of age ($n = 9$, 7, 11 and 9 for fl/fl LF, CS-Mpc2$^{-/-}$ LF, fl/fl KD and CS-Mpc2$^{-/-}$ KD, respectively). **e**, Survival curve of LF- or KD-fed mice (initial $n = 19$, 15, 21 and 14 for fl/fl LF, CS-Mpc2$^{-/-}$ LF, fl/fl KD and CS-Mpc2$^{-/-}$ KD, respectively). **f**, Representative short-axis H&E images and magnified trichrome stains of hearts from LF- or KD-fed 17-week-old mice (black scale bar, 1 mm; white scale bars, 20 μm; similar data reproduced with seven independent groups of littermate mice). **g,h**, Heart weight (HW) (**g**) and lung weight (**h**) normalized to tibia length (TL) of LF- or KD-fed 17-week-old mice ($n = 19$, 11, 20 and 14 for fl/fl LF, CS-Mpc2$^{-/-}$ LF, fl/fl KD and CS-Mpc2$^{-/-}$ KD, respectively). **i**, Cardiac myocyte CSA measured from H&E images ($n = 8$, 5, 9 and 7 for fl/fl LF, CS-Mpc2$^{-/-}$ LF, fl/fl KD and CS-Mpc2$^{-/-}$ KD, respectively). **j–n**, Gene expression markers of cardiac hypertrophy/failure and fibrosis (*Nppa* (**j**), *Nppb* (**k**), *Acta1* (**l**), *Col1a1* (**m**) and *Col3a1* (**n**)) from mouse hearts ($n = 7$, 5, 6 and 6 for fl/fl LF, CS-Mpc2$^{-/-}$ LF, fl/fl KD and CS-Mpc2$^{-/-}$ KD, respectively). **o**, Western blot images for signalling pathways associated with cardiac hypertrophic growth (phospho-ERK, total ERK, phospho-AMPKα, total AMPKα, phospho-mTOR, total mTOR, phospho-S6-ribosomal protein, total S6-ribosomal protein and β-actin) from hearts of LF- or KD-fed mice ($n = 3$). Mean ± s.e.m. shown within dot plots. Each symbol represents an individual sample. Two-way ANOVA with Tukey's multiple-comparisons test.

also fed fl/fl and CS-MPC2$^{-/-}$ mice two diets that were higher in fat, but with moderate levels of carbohydrate and protein, which only modestly increased plasma ketone body concentrations compared to LF-fed fl/fl mice (Fig. 6a,b). Feeding CS-MPC2$^{-/-}$ mice a ~42% medium-chain triglyceride (MCT) or a 60% HF diet was able to significantly improve cardiac enlargement and contractile function as measured by echocardiography (Fig. 6c,d, Extended Data Fig. 6a–i and Supplementary Video 2). Heart weight, lung oedema

and hypertrophic/fibrotic gene expression were also significantly improved by MCT and HF diets (Fig. 6e–m). In CS-MPC2$^{-/-}$ hearts the HF diet was also capable of enhancing expression of *Ppara* and its target genes (Extended Data Fig. 6j–l), as well as lowering *Bdh1* expression (Fig. 6n) compared to LF diet. Thus, diets enriched with higher levels of fat but enough carbohydrate and protein to limit ketosis were also able to significantly improve or even prevent cardiac remodelling and dysfunction in CS-MPC2$^{-/-}$ mice.
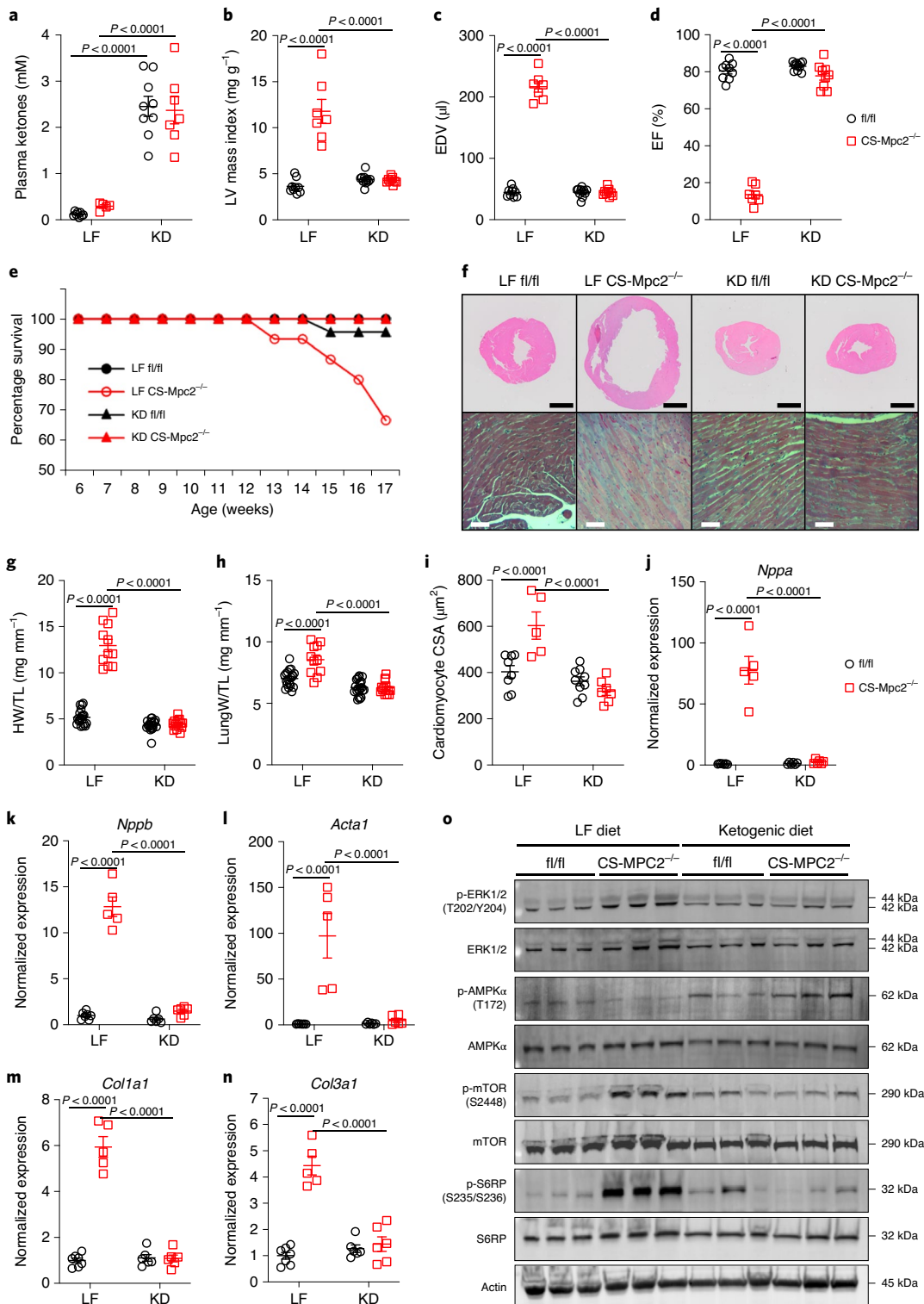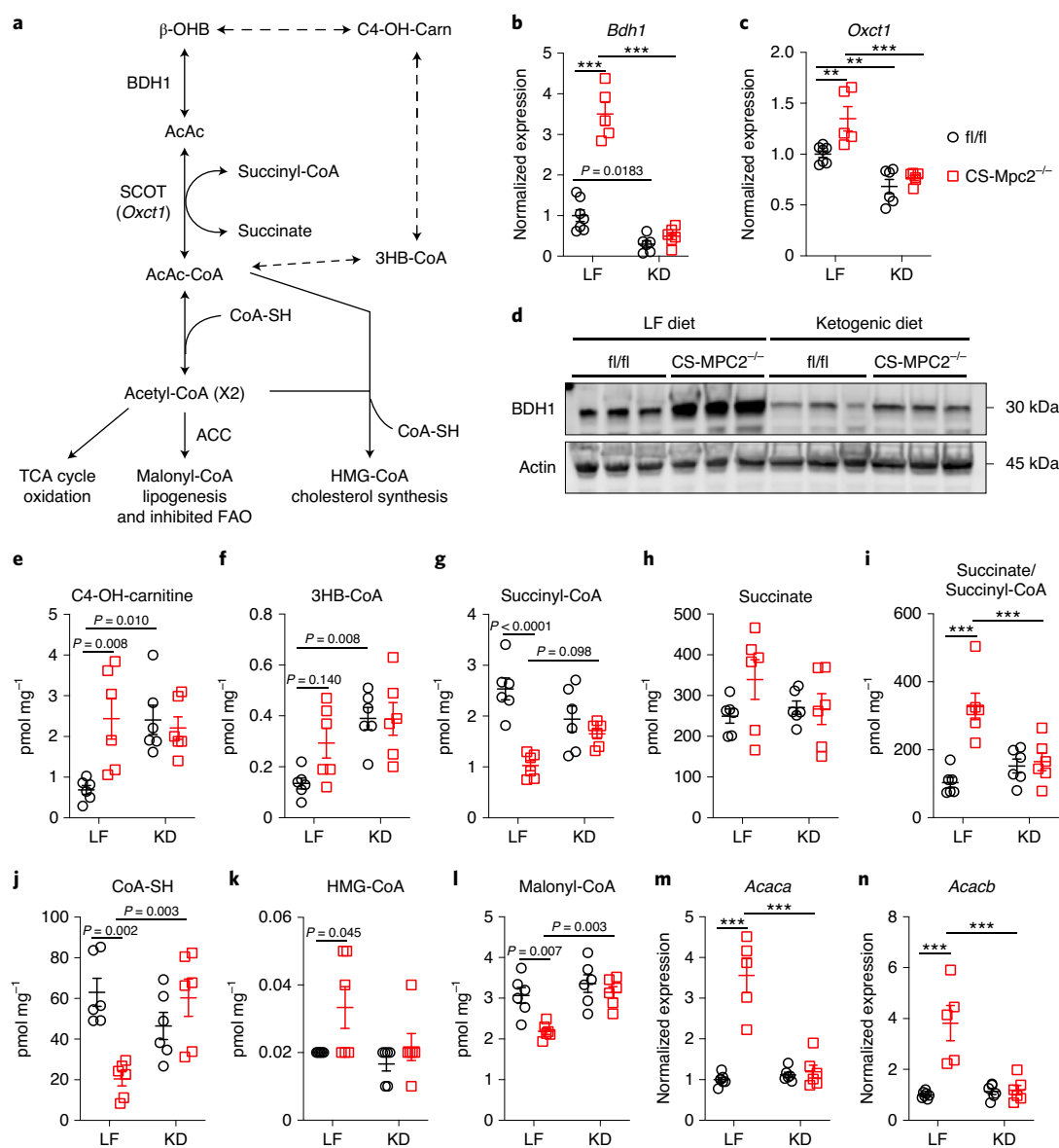
Fig. 4 | KD downregulates cardiac ketone body catabolism. a, Schematic of oxidative and nonoxidative ketone body catabolism. **b,c**, Gene expression of *Bdh1* and *Oxct1* from hearts of LF- or KD-fed fl/fl or CS-Mpc2$^{-/-}$ mice ($n = 7, 5, 6$ and 6 for fl/fl LF, CS-Mpc2$^{-/-}$ LF, fl/fl KD and CS-Mpc2$^{-/-}$ KD, respectively) (*Oxct1*: $P = 0.0058$ for LF fl/fl versus CS-Mpc2$^{-/-}$, $P = 0.0083$ for fl/fl LF versus KD). **d**, Western blot images of BDH1 and Actin from heart tissue of LF- or KD-fed mice ($n = 3$). **e–l**, Cardiac concentrations of metabolites associated with ketone body catabolism (C4-OH-carnitine (**e**), 3HB-CoA (**f**), succinyl-CoA (**g**), succinate (**h**), succinate/succinyl-CoA ratio (**i**), free CoA-SH (**j**), HMG-CoA (**k**) and malonyl-CoA (**l**)) measured in hearts from LF- or KD-fed mice ($n = 6$). **m,n**, Gene expression for *Acaca* (**m**) and *Acacb* (**n**) normalized to *Rplp0* from hearts of LF- and KD-fed mice ($n = 7, 5, 6$ and 6 for fl/fl LF, CS-Mpc2$^{-/-}$ LF, fl/fl KD and CS-Mpc2$^{-/-}$ KD, respectively). Mean ± s.e.m. shown within dot plots. Each symbol represents an individual sample. Two-way ANOVA with Tukey's multiple-comparisons test. *$P < 0.05$, **$P < 0.01$, ***$P < 0.001$.

A 24-h fast improves cardiac remodelling concordant with enhanced fat oxidation. Like KD, prolonged fasting increases the cardiac reliance on FAO and reduces ketolytic flux despite increased cardiac ketone body delivery[35]. We aged fl/fl and CS-MPC2$^{-/-}$ mice to 16 weeks, and then either fasted them for 24 h or allowed them to continue consuming chow ad libitum. As expected, the 24 h fast reduced blood glucose levels, and strongly enhanced plasma concentrations of nonesterified fatty acids and ketone bodies in both fl/fl and CS-MPC2$^{-/-}$ mice (Fig. 7a–c). Fasting completely corrected the elevated blood lactate concentrations (Extended Data Fig. 7a), but had no effect on the elevated cardiac glycogen concentrations observed in fed CS-MPC2$^{-/-}$ mice (Extended Data Fig. 7b). Fasting

also did not markedly alter plasma triacylglycerol concentrations (Extended Data Fig. 7c). The 24 h fast significantly improved CS-MPC2$^{-/-}$ heart weights (Fig. 7d) and several gene expression markers of hypertrophy, failure and fibrosis (Fig. 7e–g and Extended Data Fig. 7d–e). Similar to KD feeding, despite mM concentrations of circulating ketone bodies, 24 h fasting resulted in reduced expression of the ketolytic enzymes *Bdh1* and *Oxct1* in the heart compared to the fed condition (Fig. 7h–i). While many PPARα target genes and genes important for FAO, including *Cpt1b*, *Acadl* and *Acadm*, were reduced in the fed CS-MPC2$^{-/-}$ hearts, these were all normalized or even enhanced by the 24 h fast (Fig. 7j–l and Extended Data Fig. 7f–h). *Acaca*, which encodes acetyl-CoA carboxylase and
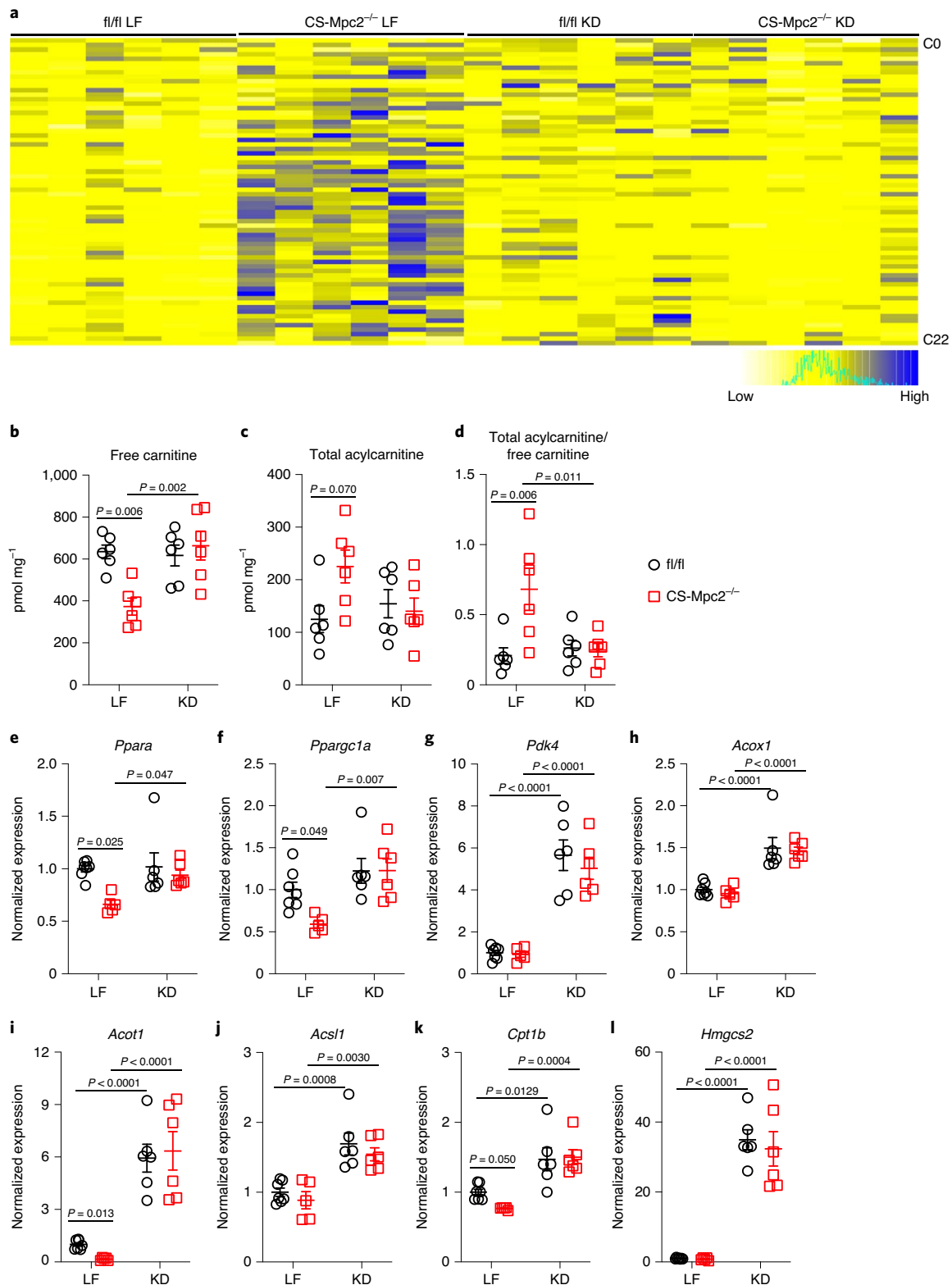
Fig. 5 | KD enhances cardiac fatty acid metabolism. a, Heatmap of acylcarnitine species measured in hearts of LF- or KD-fed fl/fl or CS-Mpc2$^{-/-}$ mice ($n = 6$). **b–d**, Concentrations of free carnitine (**b**), total acylcarnitines (**c**) and the acylcarnitine/free carnitine ratio (**d**) measured by mass spectrometry of heart tissue ($n = 6$). **e–l**, Gene expression markers of PPARα and FAO (*Ppara* (**e**), *Ppargc1a* (**f**), *Pdk4* (**g**), *Acox1* (**h**), *Acot1* (**i**), *Acsl1* (**j**), *Cpt1b* (**k**) and *Hmgcs2* (**l**)) from heart tissue of LF- or KD-fed mice ($n = 7$, 5, 6 and 6 for fl/fl LF, CS-Mpc2$^{-/-}$ LF, fl/fl KD and CS-Mpc2$^{-/-}$ KD, respectively). Mean ± s.e.m. shown within dot plots. Each symbol represents an individual sample. Two-way ANOVA with Tukey's multiple-comparisons test.

generates malonyl-CoA, which inhibits mitochondrial fat oxidation, was elevated in the fed CS-MPC2$^{-/-}$ hearts and reduced by fasting (Extended Data Fig. 7i).

A subset of hearts were used to generate permeabilized cardiac muscle fibres to assess their ability to oxidize pyruvate and palmitoyl-CoA. As expected, the CS-MPC2$^{-/-}$ heart fibres
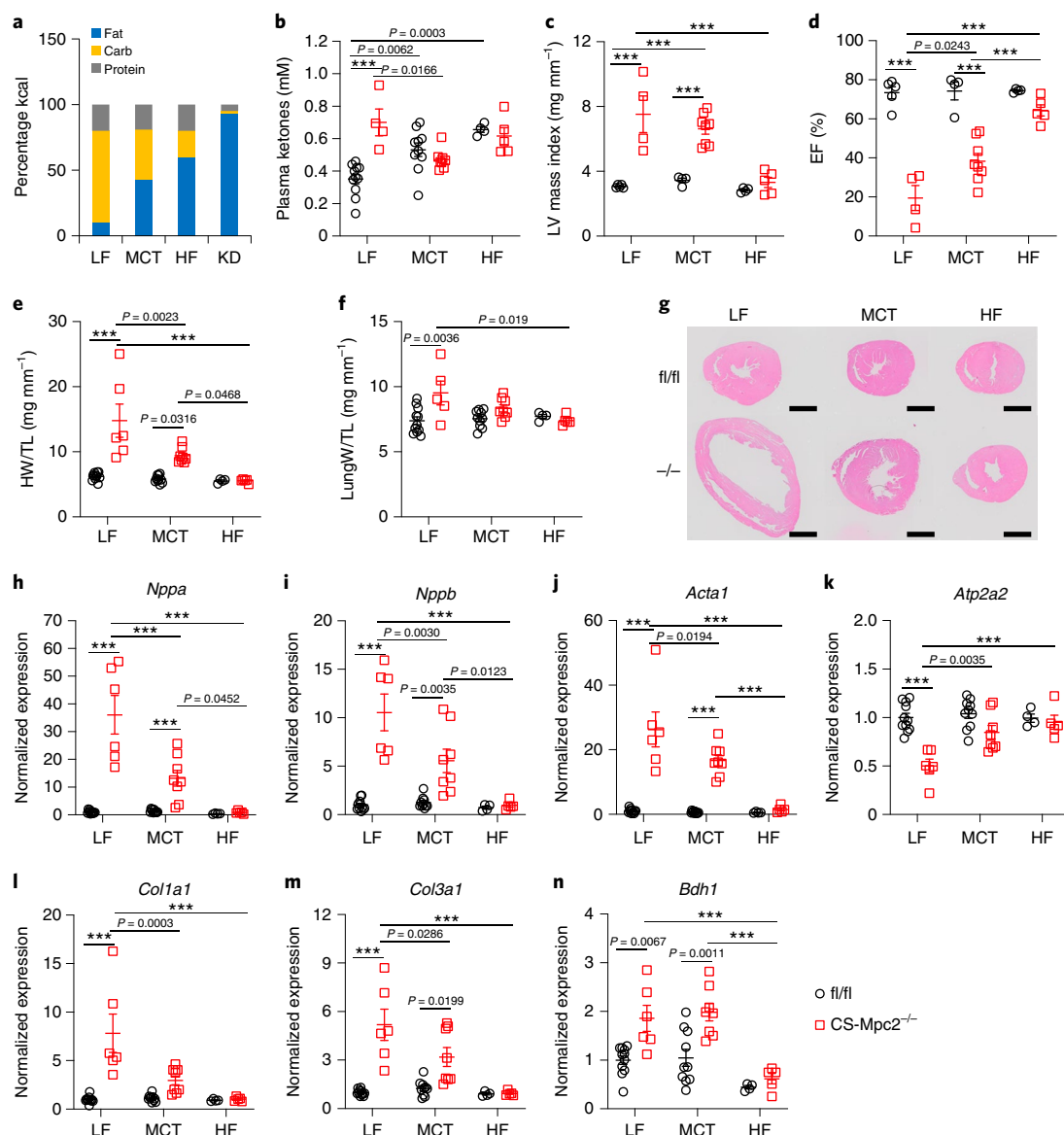
Fig. 6 | HF diets also prevent cardiac remodelling and dysfunction in CS-MPC2⁻/⁻ mice. a, Comparison of diet macronutrient composition for LF, MCT, HF and KD. **b**, Plasma total ketone body concentrations measured from mice after LF, MCT or HF diet feeding (n = 11, 4, 10, 8, 4 and 5 for fl/fl LF, CS-Mpc2⁻/⁻ LF, fl/fl MCT, CS-Mpc2⁻/⁻ MCT, fl/fl HF and CS-Mpc2⁻/⁻ HF, respectively). **c,d**, Echocardiography measures of LV mass index (**c**) and ejection fraction (EF) (**d**) of mice fed LF, MCT or HF diets (n = 5, 4, 4, 8, 4 and 5 for fl/fl LF, CS-Mpc2⁻/⁻ LF, fl/fl MCT, CS-Mpc2⁻/⁻ MCT, fl/fl HF and CS-Mpc2⁻/⁻ HF, respectively). **e,f**, Heart weight (HW) (**e**) and lung weight (**f**) normalized to tibia length (n = 11, 6, 10, 8, 4 and 5 for fl/fl LF, CS-Mpc2⁻/⁻ LF, fl/fl MCT, CS-Mpc2⁻/⁻ MCT, fl/fl HF and CS-Mpc2⁻/⁻ HF, respectively). **g**, Representative short-axis heart images stained with H&E (scale bar, 1 mm; similar results obtained during four independent experiments of littermate mice). **h–n**, Gene expression markers of hypertrophy, heart failure and fibrosis (*Nppa* (**h**), *Nppb* (**i**), *Acta1* (**j**), *Atp2a2* (**k**), *Col1a1* (**l**) and *Col3a1* (**m**)) and the ketolytic-enzyme-encoding gene *Bdh1* (**n**) from mouse hearts (n = 11, 6, 10, 8, 4 and 5 for fl/fl LF, CS-Mpc2⁻/⁻ LF, fl/fl MCT, CS-Mpc2⁻/⁻ MCT, fl/fl HF and CS-Mpc2⁻/⁻ HF, respectively). Mean ± s.e.m. shown within dot plots. Each symbol represents an individual sample. Two-way ANOVA with Tukey's multiple-comparisons test. Exact *P* values given unless ***P < 0.0001.

displayed lower OCR from pyruvate in both the fed and fasted conditions (Fig. 7m). Fasting reduced pyruvate-stimulated respiration in the fl/fl hearts and also tended to reduce OCR from pyruvate in the CS-MPC2⁻/⁻ hearts. In the fed condition, failing CS-MPC2⁻/⁻ hearts displayed reduced OCR with palmitoyl-CoA as substrate during both state 2 and ADP-stimulated state 3 conditions (Fig. 7n,o). However, palmitoyl-CoA respiration was strongly enhanced in the CS-MPC2⁻/⁻ hearts by the 24 h fast (Fig. 7n,o). In summary, a 24 h fast significantly reduced the size of CS-MPC2⁻/⁻ hearts and suppressed the expression of hypertrophic and fibrotic

genes, which was associated with a downregulation of ketolytic enzymes and an enhancement of cardiac fat oxidation.

KD can reverse heart failure in CS-MPC2⁻/⁻ mice. We also assessed whether 3 weeks of feeding the HF, low-carbohydrate KD could reverse existing heart failure. We allowed CS-MPC2⁻/⁻ mice to consume chow until 16 weeks of age, then assigned them to either LF or KD feeding for 3 weeks (Fig. 8a). All CS-MPC2⁻/⁻ mice displayed cardiac dilation and poor contractile function during the 16-week echocardiograms, which remained or were worsened after
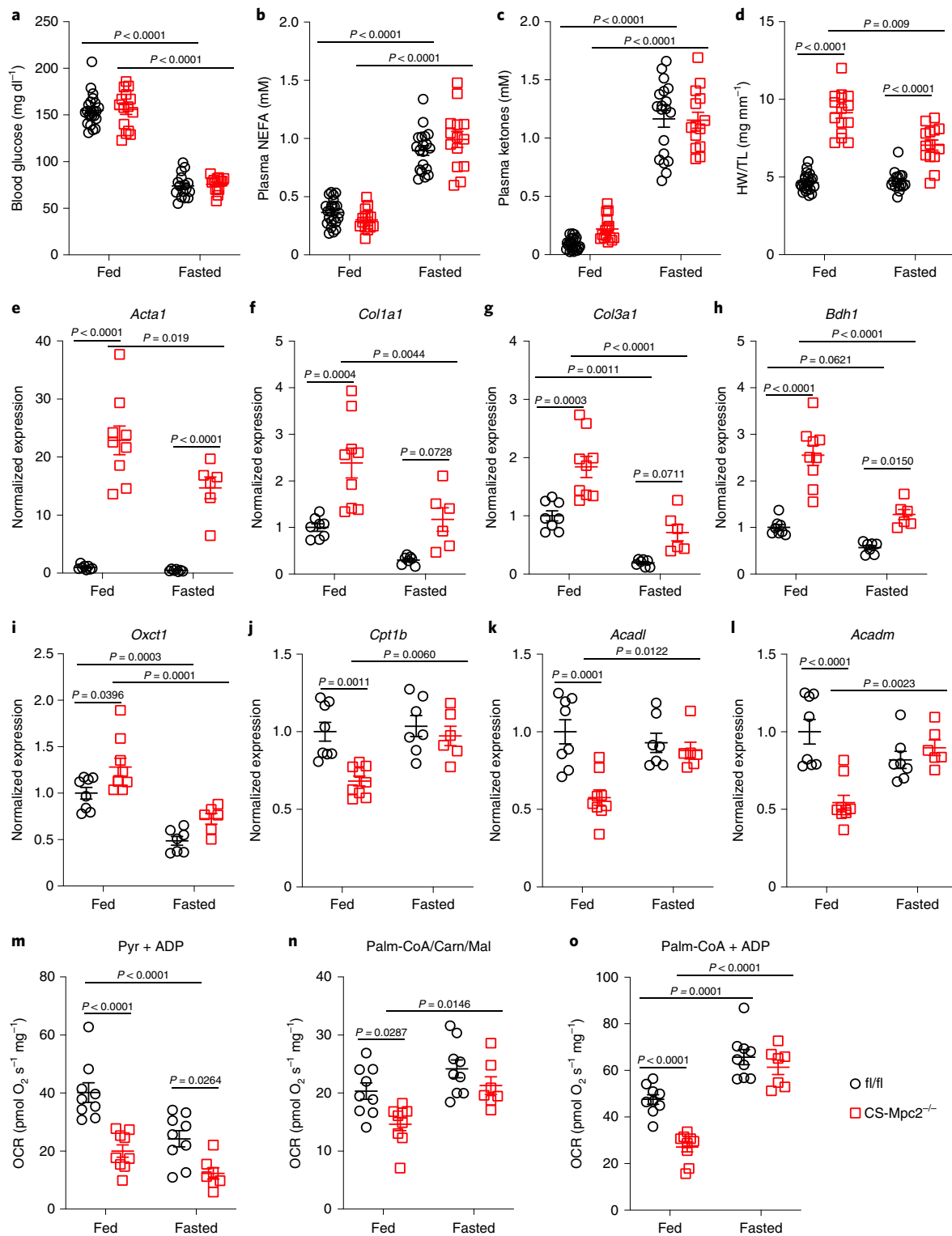
Fig. 7 | Improved cardiac remodelling during fasting is associated with enhanced fat oxidation. a–c, Blood glucose (**a**), plasma nonesterified fatty acid (NEFA) (**b**) and plasma total ketone body concentrations (**c**) from fed or 24 h-fasted mice (n = 22, 15, 16 and 14 for fl/fl fed, CS-Mpc2$^{-/-}$ fed, fl/fl fasted and CS-Mpc2$^{-/-}$ fasted, respectively). **d**, Heart weight normalized to tibia length after feeding or fasting (n = 22, 15, 16 and 14 for fl/fl fed, CS-Mpc2$^{-/-}$ fed, fl/fl fasted and CS-Mpc2$^{-/-}$ fasted, respectively). **e–l**, Cardiac gene expression markers of heart failure, fibrosis, or ketone- and fatty acid–metabolizing enzymes (Acta1 (**e**), Col1a1 (**f**), Col3a1 (**g**), Bdh1 (**h**), Oxct1 (**i**), Cpt1b (**j**), Acadl (**k**) and Acadm (**l**)) (n = 8, 9, 7 and 6 for fl/fl fed, CS-Mpc2$^{-/-}$ fed, fl/fl fasted and CS-Mpc2$^{-/-}$ fasted, respectively). **m–o**, OCRs measured from permeabilized cardiac muscle fibres by using pyruvate (Pyr) + ADP (**m**) or palmitoyl-CoA with carnitine and malate (Palm-CoA/Carn/Mal), before (**n**) and after (**o**) addition of ADP (n = 9, 9, 9 and 7 for fl/fl fed, CS-Mpc2$^{-/-}$ fed, fl/fl fasted and CS-Mpc2$^{-/-}$ fasted, respectively). Data are presented as mean ± s.e.m. within dot plots. Each symbol in the dot plots represents an individual sample. Two-way ANOVA with Tukey's multiple-comparisons test.
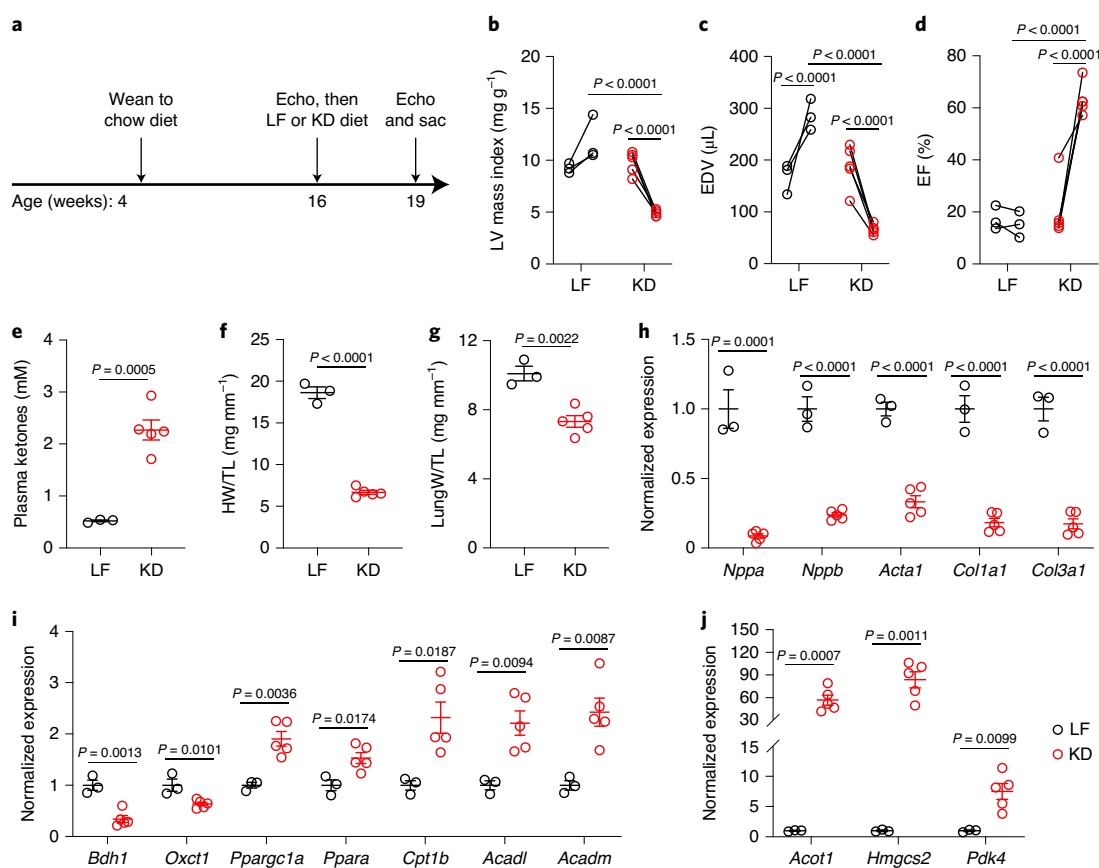
Fig. 8 | KD can reverse heart failure in CS-Mpc2$^{-/-}$ mice. a, Timeline for heart failure reversal experiment, in which CS-MPC2$^{-/-}$ mice were switched to LF or KD at 16 weeks of age for 3 weeks. **b–d**, Echocardiography measures of LV mass index (**b**), end-diastolic volume (EDV) (**c**) and ejection fraction (EF) (**d**) of CS-MPC2$^{-/-}$ mice pre- and post-LF or KD feeding ($n=3$ LF, 5 KD; data presented as pre–post with first data point at 16 weeks old and second data point at 19 weeks old after 3 weeks of LF or KD). **e**, Plasma total ketone values from CS-MPC2$^{-/-}$ mice fed LF or KD ($n=3$ LF, 5 KD). **f,g**, Heart weight (HW) (**f**) and lung weight (**g**) normalized to tibia length ($n=3$ LF, 5 KD). **h–j**, Cardiac gene expression of hypertrophy, heart failure, fibrosis (*Nppa, Nppb, Acta1, Col1a1* and *Col3a1*; **h**), ketone body– and fatty acid–metabolism genes (*Bdh1, Oxct1, Ppargc1a, Ppara, Cpt1b, Acadl* and *Acadm*; **i**) and PPARα target genes (*Acot1, Hmgcs2* and *Pdk4*; **j**) ($n=3$ LF, 5 KD). Data presented either as pre–post, or mean ± s.e.m. shown within dot plots. Each symbol represents an individual sample. Two-tailed paired Student's *t*-test to compare pre versus post, two-tailed unpaired Student's *t*-test to compare LF versus KD.

3 weeks of LF diet feeding (Fig. 8b–d and Extended Data Fig. 8a–h). However, 3 weeks of KD feeding greatly improved the LV dilation and contractile function of the previously failing CS-MPC2$^{-/-}$ hearts (Fig. 8b–d, Extended Data Fig. 8a–h and Supplementary Video 3). The 3 weeks of KD feeding strongly elevated ketosis (Fig. 8e) and heart weight, lung oedema and cardiac gene expression markers of pathological remodelling and fibrosis were all drastically reversed by 3 weeks of KD feeding (Fig. 8f–h). Last, the 3 weeks of KD feeding reduced cardiac gene expression of ketolytic enzymes and induced PPARα target genes encoding fat oxidation enzymes (Fig. 8i,j). Thus, KD consumption for only 3 weeks and the concordant increase in fat metabolism was associated with reverse remodelling of the failing CS-MPC2$^{-/-}$ hearts to essentially normal size.

Discussion

Myocardial fuel metabolism is altered in hypertrophy and heart failure, characterized as a generalized decrease in the ability to oxidize fatty acids and pyruvate in the mitochondria[17,18,38]. The import of pyruvate into the mitochondria occurs via the MPC, which was identified in 2012 as a hetero-oligomeric complex of MPC1 and MPC2 proteins[19,20]. An early study conducted before the cloning of MPC proteins and using a chemical inhibitor estimated that cardiac MPC expression was high, and MPC activity would be rate limiting

for pyruvate oxidation in heart mitochondria[39]. Subsequent studies agreed that inhibitor binding of cardiac mitochondria was very high (indicating high cardiac MPC expression), but did not suggest pyruvate transport to be the limiting factor for pyruvate oxidation[40,41]. Studies regarding the importance of MPC activity in cardiac function or development of heart failure have been limited. Expression of MPC1 and MPC2 was shown to be an important marker of surviving myocardium near the border of infarct zones in a pig model, and this study also identified increased MPC expression in human hearts with ischaemic heart failure[42]. While this current work was in preparation, another report showed that failing human hearts exhibited decreased expression of the MPC proteins[25], which we have confirmed in this current study. Thus, myocardial MPC expression in heart failure may depend on ischaemic versus nonischaemic aetiology, as well as location in relation to infarct zone. Together with two companion papers[43,44], we show that complete deletion of the MPC in myocardium leads to a severe, progressive cardiac remodelling and dilated heart failure. However, pharmacologic MPC inhibition or loss of one MPC2 allele and approximately 50% of the MPC protein did not affect cardiac function. These findings suggest that partial inhibition of MPC activity in the heart can be overcome metabolically and is not sufficient to cause pathologic remodelling as long as other cardiac stressors are not present. However, the work of

Fernandez-Caggiano and colleagues demonstrates that MPC1 over-expression in a TAC model improves hypertrophy[43], suggesting that MPC deactivation in the context of pressure overload plays a role in pathological remodelling.

Previous work has shown that modulating the expression or activity of PDH limits cardiac metabolic flexibility by decreasing glucose oxidation and increasing FAO[21–24]. These models of decreased PDH activity did not result in overt cardiac dysfunction. One possible explanation for why MPC deletion is more severe is that blocking pyruvate entry could also affect pyruvate carboxylation (anaplerosis) and the replenishing of TCA cycle intermediates. Although the effects of deleting pyruvate carboxylase in the myocardium are unknown, this pathway is known to be active in the heart[45]. However, most pyruvate carboxylation in the heart likely occurs by nicotinamide adenine dinucleotide phosphate ($NADP^+$)-dependent malic enzyme[46] generating malate in the cytosol. Additionally, the abundance of most TCA cycle metabolites was normal or even elevated in the CS-MPC2$^{-/-}$ hearts (Fig. 1g,h and Supplementary Tables 1 and 3), suggesting no defect in anaplerosis. Another possibility is that a small amount of pyruvate is able to enter the mitochondrial matrix in the absence of the MPC, potentially through pyruvate-alanine cycling as we have described in the liver[26].

The current studies cannot definitively explain why CS-MPC2$^{-/-}$ mice develop heart failure. The simplest explanation would be that an inability to oxidize pyruvate results in an energetic deficit. The failing CS-MPC2$^{-/-}$ hearts display decreased AMPK phosphorylation (Fig. 3o), suggesting that their metabolic stress does not involve dysregulated AMP/ATP levels. Another possibility is that a decrease in mitochondrial pyruvate metabolism results in an accumulation of metabolic intermediates that enhance hypertrophic signalling. One example of this would be the oncometabolite 2-hydroxyglutarate (2-HG), which has been implicated in driving cardiac hypertrophy and impairing contractility[47,48]. We found that failing LF-fed CS-MPC2$^{-/-}$ hearts contained almost twofold higher concentrations of total 2-HG (Supplementary Table 3). However, hearts from KD-fed mice also had higher total 2-HG than those from LF-fed fl/fl mice (Supplementary Table 3). Unfortunately, our mass spectrometry analyses did not distinguish between D- and L-2-HG, as only D-2-HG appears to be responsible for inducing cardiomyopathy[47,48]. Two recent studies have suggested that cardiac hypertrophy is associated with enhanced glucose flux into the pentose phosphate pathway, generating reducing equivalents as NADPH and potentially other metabolites that signal to mTOR to stimulate protein synthesis[49,50]. While we have not identified specific signals, we can confirm that the failing CS-MPC2$^{-/-}$ hearts display enhanced mTOR activation and downstream signalling to support hypertrophic growth (Fig. 3o). The decreased AMPK phosphorylation in CS-MPC2$^{-/-}$ hearts likely does not indicate 'energetic stress', but is consistent with elevated mTOR activation, as AMPK is a repressor of mTOR activity. However, the relationship between AMPK and cardiac hypertrophy is not completely clear, as genetic mouse models of AMPK depletion do not lead to hypertrophy[51,52] and can even protect against isoproterenol-induced hypertrophy[53]. Additionally, while acute pharmacologic AMPK activation inhibits mTOR, chronic AMPK activation can induce cardiac hypertrophy[54]. Last, a recent study also showed that enhancing fat oxidation via acetyl-CoA carboxylase 2 deletion was able to reduce altered glucose metabolism and prevent cardiac hypertrophy[50]. Therefore, as our current study suggests, altered glucose and pyruvate metabolism seems to drive pathologic remodelling, while enhanced fat oxidation appears to correct this cardiac remodelling. Further study is required to dissect what metabolites are altered by decreased MPC activity that ultimately increase hypertrophic growth.

Recent studies have described improvements in cardiac function with ketone body infusion in both a dog model and human patients with heart failure[33,55]. Additionally, genetic mouse models of BDH1 or OXCT1 suggest that increased ketone metabolism is a protective adaptation in heart failure[33,56,57]. A KD was unable to improve cardiac hypertrophy in a mouse model of defective FAO caused by carnitine palmitoyltransferase 2 deletion[58], suggesting that enhancing ketolysis per se cannot rescue heart failure in that model. Several lines of evidence suggest that the prevention or reversal of heart failure in CS-MPC2$^{-/-}$ mice were driven by enhanced fatty acid metabolism rather than ketone body use. Injecting CS-MPC2$^{-/-}$ mice daily with β-hydroxybutyrate did slightly ameliorate cardiac remodelling, but feeding a ketone ester-supplemented chow did not improve cardiac size or function. Diets that were enriched with fat, but were not overtly ketogenic, were also able to significantly prevent heart failure in CS-MPC2$^{-/-}$ mice. While hearts can extract and metabolize ketone bodies in proportion to their delivery, ketones and fatty acids are in competition for oxidation[7–9] and in agreement with a previous report in normal mouse hearts[35], we show that fasting or KD decreased the expression of the ketolytic enzymes BDH1 and OXCT1 and likely reduced ketolytic flux. KD feeding and fasting were also associated with upregulation of PPARα-target genes related to FAO and corrected the cardiac accumulation of acylcarnitines. Fasted CS-MPC2$^{-/-}$ hearts also displayed increased oxidation of palmitoyl-CoA consistent with enhanced fat oxidation.

It should also be noted that the MPC has been suggested to also be a mitochondrial importer/exporter of ketone bodies[59], which may further suggest that the ameliorative effects of KD on MPC hearts are not due to enhanced cardiac ketolysis. However, there is genetic evidence that the MPC is not the sole mitochondrial ketone transporter. Cardiac β–hydroxybutyrate flux into the TCA cycle was actually increased in MPC1$^{-/-}$ hearts[44], indicating that the MPC is not required for cardiac mitochondrial ketone body import. Ketone bodies are produced and released almost exclusively in the liver, and hepatic MPC1/2 knockout mice display normal or even enhanced plasma ketone body concentrations[26,60], suggesting no defect in mitochondrial ketone export. Whether genetic loss of the MPC affects mitochondrial ketone import/export will require future study.

Last, it is interesting that the degree of heart failure improvement appears to also track with a reduction in dietary carbohydrate. Hearts from CS-MPC2$^{-/-}$ mice showed even worse failure after refined LF diet feeding compared to chow feeding (Fig. 3 and Extended Data Fig. 3 compared to Fig. 2 and Extended Data Fig. 2), potentially due to the large amount of sucrose in the LF diet compared to complex carbohydrates in chow. Fasting also lowered blood glucose concentrations and is known to reduce cardiac glucose uptake and oxidation[35]. Collectively, we believe the present data using a variety of model systems suggest that enhanced FAO and limiting the provision of carbohydrate to be the predominant mechanism for preventing or reversing cardiac dysfunction in CS-MPC2$^{-/-}$ mice.

In conclusion, these studies describe that the MPC is deactivated in failing human and mouse hearts and that cardiac deletion of MPC2 in mice results in progressive cardiac hypertrophy and dilated heart failure. Heart failure in CS-MPC2$^{-/-}$ mice could be prevented or even reversed by feeding a KD, and an acute fast was also able to initiate reverse remodelling. These improvements appear to be predominantly mediated by increasing cardiac fat oxidation and limiting provision of carbohydrate, rather than enhancing ketone metabolism. Some mechanistic aspects of the cause of heart failure observed in mice lacking MPC in the heart remain to be teased apart. A limitation of the models we used is that the circulating ketone concentrations generated by ketone injection or feeding ketone ester diet are not as high as when feeding a KD or fasting. Thus, it is difficult to say whether a more pronounced level of ketosis would also improve the CS-MPC2$^{-/-}$ hearts.

Methods

Human heart tissue collection. Human heart tissue was collected with written informed consent received from participants as part of an Institutional Review Board (IRB)-approved protocol (no. 201101858) at the Washington University School of Medicine. Failing human LV heart tissue was obtained from the Washington University Translational Cardiovascular Tissue Core at the time of LVAD placement or post-LVAD placement at the time of cardiac transplantation. Nonfailing human heart tissue was obtained from Mid-America Transplant from hearts deemed unsuitable for transplantation due to donor age, nonocclusive coronary artery disease or high-risk behavioural profile. The collected piece of cardiac tissue had fat removed, was rinsed in saline, then snap frozen in liquid nitrogen and stored at −80 °C until analysis.

Animals. All animal procedures were performed in accordance with National Institutes of Health (NIH) guidelines and approved by the Institutional Animal Care and Use Committees at the Washington University School of Medicine and Saint Louis University School of Medicine (Protocol 2845). The use of mice conformed to guidelines set out by the NIH[61]. Generation of mice with the *Mpc2* gene flanked by loxP sites has been described previously[26]. To create cardiac myocyte specific deletion, these mice were crossed with a knock-in mouse in which one allele of the myosin light chain 2v gene (*Myl2*) was replaced with Cre recombinase[62], which was obtained from the Jackson Laboratory. This Mlc2vCre mouse was on the C57BL/6J background (Jackson Laboratory Stock no. 029465). All mice used in these studies were from a C57BL6/J background. Unless specifically noted, all experiments were performed with a mixture of male and female littermate mice. Most studies were performed with mice beginning at 6 weeks old and ending at 16–17 weeks of age (chow, KD study and MCT/HFD study). The fed/fasted study was performed on mice that were chow fed for 16 weeks before an acute 24 h fast. For the KD reversal study, 16-week-old chow-fed mice were switched to either LF or KD for 3 weeks and euthanized at 19 weeks of age. For the TAC + MI studies, 4–5-week-old WT C57BL6/J females were purchased from the Jackson Laboratory and thus were not necessarily littermates.

Animal care. Mice were housed in a climate-controlled barrier facility maintained at 22–24 °C and 40–60% humidity in ventilated cages with a 12-h light/dark cycle with light period from 6:00 to 18:00 local time. Ad libitum access to drinking water was provided by individual bottles in each cage. Mice were housed in cages with corn-cob bedding or switched to aspen chip bedding during special diet studies or fasting before killing. All mice were group-housed, up to five mice per cage, with cloth nestlets to use for enrichment. Mice on special diets were also provided with a Nylabone (Central Garden and Pet Co.) for both enrichment and to maintain teeth when fed soft, higher fat diets. With all diets, mice were provided ad libitum access to food, except for a brief 4-h fast before euthanasia. Unless specifically noted, all special diets were initiated at 6 weeks of age. All diets were provided on a wire rack above the cage bedding, with the exception of the KD paste, which was spread into a glass Petri dish, placed on the bottom of the cage and replaced every 2–3 d. Mice fed standard chow received PicoLab Rodent Diet 20 (no. 5053, LabDiet) consisting of 62.1%kcal carbohydrate, 13.2%kcal fat and 24.7%kcal protein. The refined LF diet was composed of 70%kcal carbohydrate, 10%kcal fat and 20%kcal protein (D12450B, Research Diets). The HF, low-carbohydrate, low protein KD was composed of 1.8%kcal carbohydrate, 93.4%kcal fat and 4.7%kcal protein (F3666, Bio-Serv). The MCT diet was composed of 37.9%kcal carbohydrate, 43%kcal fat (depleted of long-chain fatty acids) and 19.1%kcal protein (TD.00308, Envigo). The HF diet was composed of 20%kcal carbohydrate, 60%kcal fat and 20%kcal protein (D12492, Research Diets). Hearts were also analysed from a cohort of WT mice fed a high trans-fat, fructose, cholesterol (HTF-C) diet (D09100301, Research Diets) with or without insulin-sensitizing MPC inhibitor MSDC-0602K treatment, which were previously described with respect to nonalcoholic steatohepatitis[28]. For the ketone ester diet experiment, control diet consisted of 63%kcal carbohydrate, 10%kcal fat and 24%kcal protein (104403, Dyets), and the ketone ester diet was composed of the same diet except 16.5%kcal of the carbohydrates was replaced with D-β-hydroxybutyrate-(R)-1,3 butanediol monoester 'ketone ester' (16.5%kcal ketone ester, 46.5%kcal carbohydrate, 10%kcal fat and 24%kcal protein) (104404, Dyets). Control or ketone ester diet were fed from 9–15 weeks of age.

Unless specifically noted, mice were euthanized after a 4-h fast by CO_2 asphyxiation and blood was collected via cannulation of the inferior vena cava into EDTA-treated tubes. Tissues were then excised, rinsed in PBS, weighed and snap frozen in liquid nitrogen. Plasma was collected by spinning blood tubes at 8,000*g* for 8 min and then freezing the plasma supernatant in liquid nitrogen. For the fed versus 24 h-fasted experiment, 16-week-old fl/fl and CS-MPC2−/− mice were either fasted at roughly 8:00, or allowed to continue feeding on normal chow ad libitum. The following day at roughly 8:00, mice were euthanized by CO_2 asphyxiation and blood and tissue collected as above, except for a small piece of LV tissue that was processed for tissue respiration studies as explained below.

Gene expression analysis. Levels of gene expression were determined by qPCR. Total RNA was extracted from snap frozen tissues using RNA-Bee (Tel-Test). Then ~50 mg of tissue was homogenized in RNA-Bee for 3–5 min using a 3-mm stainless steel bead at 30 Hz using a TissueLyser II (Qiagen). RNA abundance and quality were assessed by Nanodrop (Thermo Fisher Scientific). Next, 1 µg of sample was reverse transcribed into complementary DNA by Superscript VILO (Thermo Fisher Scientific) using an Eppendorf Mastercycler X50 thermocycler. Relative quantification of target gene expression was measured in duplicate using Power SYBR Green (Thermo Fisher Scientific), using an ABI 7500 Real-Time PCR System (Thermo Fisher Scientific). Target gene threshold cycle (Ct) values were normalized to reference gene (*Rplp0*) Ct values by the $2^{-\Delta\Delta Ct}$ method. Oligonucleotide primer sequences used for qPCR are listed in Supplementary Table 4.

Western blotting and protein expression analysis. Protein extracts were prepared by homogenizing ~50 mg of frozen tissue in an NP-40-based lysis buffer (15 mM NaCl, 25 mM Tris base, 1 mM EDTA, 0.2% NP-40, 10% glycerol) supplemented with 1× cOmplete protease inhibitor cocktail (Roche) and a phosphatase inhibitor cocktail (1 mM Na_3VO_4, 1 mM NaF and 1 mM PMSF). Tissue was homogenized in this buffer for 3–5 min using a prechilled 3-mm stainless steel bead at 30 Hz using a TissueLyser II (Qiagen). Protein concentrations were measured using a Pierce MicroBCA kit (Thermo Fisher Scientific), and detected with a BioTek Synergy plate reader and Gen5 software (BioTek Instruments). Then 50 µg of protein lysate was electrophoresed on precast Criterion 4–15% polyacrylamide gels (Biorad), and transferred onto 0.45-µm Immobilon polyvinyldifluoride membranes (MilliporeSigma). Membranes were blocked with 5% bovine serum albumin (Sigma) in Tris-buffered saline with Tween-20 (TBST) for at least 1 h.

Primary antibodies were then used at 1:1,000 (or 1:5,000 for VLCAD and LCAD) in 5%BSA-TBST overnight while rocking at 4 °C. Antibodies for human MPC1 and MPC2 were from Cell Signaling, while anti-mouse MPC1 and MPC2 antibodies were a gift from M. Wolfgang[26,63,64]. Antibodies for VLCAD[65], LCAD[66] and MCAD[67] were gifts from D. Kelly or A. Strauss. Anti-CPT1B antibody was from Alpha Diagnostic International. Anti-BDH1 and anti-OX PHOS cocktail antibodies were from Thermo Fisher Scientific. Phospho-ERK1/2 (Thr202/Tyr204), total ERK1/2, phospho-AMPKα (Thr172), total AMPKα, phospho-mTOR (Ser2448), total mTOR, phospho-S6-ribosomal protein (Ser235/236), total S6-ribosomal protein were from Cell Signaling. VDAC1 antibody was from Abcam. Anti-α-tubulin and β-actin antibodies were from Sigma. After primary antibody incubation, membranes were washed 3–5× for 5 min in TBST, and probed with IRDye secondary antibodies at 1:10,000 (Li-Cor Biosciences) in 5% BSA-TBST for 1 h. Membranes were imaged on an Odyssey imaging system and analysed with Image Studio Lite software (Li-Cor Biosciences).

Mitochondrial isolation and high-resolution respirometry. Mitochondria were isolated by differential centrifugation from whole mouse hearts by homogenization with ten passes of a glass-on-glass Dounce homogenizer on ice with 4 ml of buffer containing 250 mM sucrose, 10 mM Tris base and 1 mM EDTA (pH 7.4). Homogenates were then spun at 1,000*g* for 5 min at 4 °C to pellet nuclei and undisrupted cell debris. The supernatant was then spun at 10,000*g* for 10 min to pellet the mitochondrial fraction. The mitochondrial pellet was washed twice in homogenization buffer minus the EDTA with 10,000*g* 10-min spins. After the final wash, mitochondrial pellets were solubilized in ~150 µl of Mir05 respiration buffer (0.5 mM EGTA, 3 mM $MgCl_2$, 60 mM lactobionic acid, 20 mM taurine, 10 mM KH_2PO_4, 20 mM HEPES, 110 mM sucrose and 1 g l−1 of fatty acid free bovine serum albumin; pH 7.1). Mitochondrial protein concentration was then measured using a Pierce MicroBCA kit (Thermo Fisher Scientific), and detected with a Synergy plate reader and Gen5 software (BioTek Instruments).

To measure OCRs, 50 µg of mitochondrial protein was added to each 2-ml chamber of an Oxygraph O2k equipped with DatLab software (Oroboros Instruments). Substrates used to assess pyruvate-stimulated respiration were 5 mM sodium pyruvate, 2 mM malate, 2.5 mM ADP + Mg^{2+} and then 5 µM UK-5099. To assess respiration on other substrates, 50 µM palmitoyl-DL-carnitine and 2 mM malate ± 2.5 mM ADP + Mg^{2+} or 10 mM glutamate and 2 mM malate ± 2.5 mM ADP + Mg^{2+} or 5 mM succinate + 2.5 mM ADP + Mg^{2+} were used. OCRs were measured as pmol O_2 s−1 mg−1 mitochondrial protein.

For the fed versus 24 h-fasted experiment, immediately after euthanasia, hearts were briefly stored in BIOPS solution (10 mM Ca/K_2-EGTA, 5.77 mM Na_2ATP, 6.56 mM $MgCl_2$, 20 mM taurine, 15 mM Na_2 phosphocreatine, 20 mM imidazole, 0.5 mM DTT and 50 mM MES hydrate) on ice. Then 1–4 mg of LV muscle was teased apart into fibres and permeabilized with 50 µg ml−1 saponin in 2 ml of BIOPS on ice for 20 min. After permeabilization, muscle fibres were washed in 2 ml of Mir05 buffer on ice for 15 min. Muscle fibres were patted dry, weighed and added to the 2-ml chamber of an Oxygraph O2k containing Mir05 buffer supplemented with 20 mM creatine and 25 µM blebbistatin. Before chambers were sealed, O_2 was injected to hyperoxygenate the buffer (to ~375 µM) to prevent a lack of O_2 diffusion into tissue from limiting O_2 consumption rates. After chambers were sealed and baseline respiration rates equilibrated to zero, substrates were added in the following order: 2 mM carnitine, 2.5 mM malate, 50 µM palmitoyl-CoA, 7 mM ADP + Mg^{2+}, 5 mM sodium pyruvate and 5 mM succinate. OCRs were measured as pmol s−1 mg−1 tissue weight.

Blood and plasma metabolite and hormone measurements. Immediately before euthanasia, a snip of the tail was made with a razor blade and a drop of

mixed venous blood was used to measure blood glucose using a Contour Next EZ (Bayer Ascensia Diabetes Care) glucometer. A second drop of blood was then used to measure blood lactate concentrations using a Lactate Plus meter (Nova Biomedical). Plasma insulin concentrations were measured from 10 μl of plasma by Singulex Erenna assay (Sigma) performed by the Washington University Core Laboratory for Clinical Studies. Total ketone bodies were measured from 4 μl of plasma using the Total Ketone AutoKit (FujiFilm) according to kit directions. Optical density (OD) values at 405 and 600 nm were measured every minute for 5 min, and absorbance changes were normalized to a 300 μM standard. Nonesterified 'free' fatty acids were measured from 2 μl of plasma using a nonesterified fatty acid kit according to manufacturer's directions (FujiFilm). OD at 560 nm was measured and normalized to a standard curve. Triglycerides were measured from 5 μl of plasma using Infinity assay kit according to the manufacturer's directions (Thermo Fisher Scientific). OD at 540 nm was measured and related to the OD of a standard curve. OD for all assays was measured in clear 96-well plates using a Synergy plate reader and Gen5 software (BioTek Instruments).

Targeted metabolomics for amino acids, acylcarnitines, organic acids and short chain acyl-CoAs. Mice used for targeted metabolomic analyses were fasted for 3 h, anaesthetized with 100 μg g^{-1} sodium pentobarbital injected i.p., and euthanized by excision of the beating heart. Hearts were snap frozen in liquid nitrogen and stored at −80 °C until they were collectively processed and analysed. Flash frozen hearts were pulverized to a fine powder in a liquid nitrogen chilled percussion mortar and pestle and weighed into prechilled 2-ml tubes. A chilled 5-mm homogenizing bead was added to samples and tissue was diluted to 50 mg ml^{-1} with 50% acetonitrile containing 0.3% formate (for acylcarnitines, amino acids and organic acids) or isopropanol/phosphate buffer (for CoAs), homogenized for 2 min at 30 Hz using a TissueLyser II (Qiagen) and aliquoted for metabolite assays. For all metabolite analyses, tissues and homogenates were kept on ice, centrifuged at 4 °C and when ready to measure, were placed in an autosampler kept at 4 °C.

Amino acids and acylcarnitines were analysed by flow injection electrospray ionization tandem mass spectrometry and quantified by isotope or pseudo-isotope dilution similar to previously described procedures[68–70], which are based on methods developed for fast ion bombardment tandem mass spectrometry[71]. Extracted heart samples were spiked with a cocktail of heavy-isotope internal standards (Cambridge Isotope Laboratories, or CDN Isotopes) and deproteinated with methanol. The methanol supernatants were dried and esterified with either acidified methanol or butanol for acylcarnitine or amino acid analysis, respectively. Mass spectra for acylcarnitine and amino acid esters were obtained using precursor ion and neutral loss scanning methods, respectively. The spectra were acquired in a multi-channel analyser mode to improve signal-to-noise. The data were generated using a Waters triple quadrupole detector equipped with Acquity UPLC (ultrahigh-performance liquid chromatography) system and a data system controlled by MassLynx v.4.1 operating system (Waters). For the amino acids analysis, the mass spectrometer settings were as follows: ionization mode, positive electrospray; capillary voltage, 3.6 V; cone voltage, 14 V; extractor voltage, 2 V; radiofrequency lens voltage, 0.1 V; collision energy, 14–25 V; source temperature, 130 °C; desolvation temperature, 200 °C; desolvation gas flow, 550 l h^{-1} and cone gas flow, 50 l h^{-1}. For the acylcarnitine analysis, the mass spectrometer settings were as follows: ionization mode, positive electrospray; capillary voltage, 3.5 V; cone voltage, 25 V; extractor voltage, 2 V; radiofrequency lens voltage, 0.1 V; collision energy, 30 V; source temperature, 130 °C; desolvation temperature, 200 °C; desolvation gas flow, 550 l h^{-1} and cone gas flow, 50 l h^{-1}. Ion ratios of analyte to respective internal standard computed from centroided spectra are converted to concentrations using calibrators constructed from authentic aliphatic acylcarnitines and amino acids (Sigma and Larodan) and dialyzed foetal bovine serum (Sigma).

Organic acids were analysed by capillary gas chromatography–mass spectrometry (GC–MS) using isotope dilution techniques using Trace Ultra GC coupled to ISQ MS operating under Xcalibur v.2.2 (Thermo Fisher Scientific)[72]. The mass spectrometer settings were as follows: ionization mode, electron ionization; ion source temperature, 250 °C and the transfer line temperature, 275 °C. The supernatants of tissue homogenates were spiked with a mixture of heavy-isotope labeled internal standards and the keto acids were stabilized by ethoximation. The organic acids were acidified and extracted into ethyl acetate. The extracts were dried and derivatized with N,O-bis(trimethylsilyl) trifluoroacetamide. The organic acids were quantified using ion ratios determined from single ion recordings of fragment ions that are specific for a given analyte and its internal standard. These ratios were converted to concentrations using calibrators constructed from authentic organic acids (Sigma). The heatmap for acylcarnitines was generated by shinyheatmap[73].

Short chain acyl CoA were analysed by LC–MS/MS using a method based on a previously published report[74]. The extracts were spiked with $^{13}C_2$-acetyl-CoA, centrifuged and filtered through the Millipore Ultrafree-MC 0.1-μm centrifugal filters before being injected onto the Chromolith FastGradient RP-18e high-performance liquid chromatography column, 50 × 2 mm² (MilliporeSigma) and analysed on a Waters Xevo TQ-S triple quadrupole mass spectrometer coupled to an Acquity UPLC system (Waters). The mass spectrometer settings were as

follows: ionization mode, positive electrospray; capillary voltage, 3.7 V; cone voltage, 50 V; source offset voltage, 50 V; collision energy, 28 V; dwell time, 0.06 s; desolvation temperature, 500 °C; desolvation gas flow, 600 l h^{-1}; cone gas flow, 150 l h^{-1} and nebulizer pressure, 7 bar. The following multiple reaction monitoring transitions were monitored: acetyl-CoA, 810.2 – >303.1; $^{13}C_2$-acetyl-CoA, 812.2 – >305.1; succinyl-CoA, 868.2 – >361.1 and malonyl-CoA, 854.2 – >347.1.

Mouse echocardiography. In vivo cardiac size and function were measured by echocardiography performed with a Vevo 2100 Ultrasound System equipped with a 30-MHz linear-array transducer (VisualSonics Inc.)[75]. Mice were lightly anaesthetized by i.p. injection of 0.005 ml g^{-1} of 2% Avertin (2,2,2-tribromoethanol, Sigma). If required, one-fifth of the initial dose was given as a maintenance dose at regular intervals. Hair was removed from the left anterior chest by shaving, and mice were then placed onto a warming pad in a left lateral decubitus position. Normothermia (37 °C) was maintained and monitored by a rectal thermometer. Ultrasound gel was applied to the chest and care was taken to maintain adequate transducer contact while avoiding excessive pressure on the chest. Two-dimensional and M-mode images were obtained in the long- and short-axis views. Images were retrieved off-line and analysed using the Vevo LAB software package (VisualSonics Inc.). Measurements were averaged from three separate images for each mouse. LV volumes were calculated from M-mode measurements using standard techniques[76,77]. Immediately after completion of imaging, mice were allowed to recover from anaesthesia on a warming pad and returned to their home cage. For echocardiography during the ketone ester diet experiment, procedures were the same as above except mice were anaesthetized by 1–2% inhaled isoflurane, and imaging was performed with a Vevo 770 Ultrasound System equipped with a 30-MHz linear-array transducer (VisualSonics Inc.).

Histology. Short-axis slices of the LV were fixed in 10% neutral buffered formalin overnight and processed by the Anatomic and Molecular Pathology core laboratory of the Washington University School of Medicine or the Research Microscopy and Histology Core of the Saint Louis University School of Medicine. The short-axis heart slices were embedded in paraffin blocks and sectioned onto glass slides. Slides were then stained for either haematoxylin and eosin (H&E) or Mason's trichrome stains. Cardiomyocyte CSA was measured from H&E images of the left ventricle taken at ×10 magnification. At least three images of each heart were taken and ten myocytes per image measured. CSA was measured with ImageJ software. The individual taking images and measuring cardiomyocytes size was blinded to genotype and diet.

Body composition analysis. We carried out mouse body composition analysis using an EchoMRI 3-in-1 system (EchoMRI). Briefly, after machine calibration with an olive oil standard, conscious mice were restrained in a plastic tube and placed into the instrument bore. Fat, lean, free water and total water mass was then determined. Imaging required <5 min per mouse and, following imaging, mice were immediately placed back into their home cage.

TAC + MI surgically induced heart failure model. Here, 7-week-old female WT C57BL/6J mice (Jackson Laboratory) were subjected to TAC + MI surgery as performed previously[75,78]. Mice were anaesthetized with 100 mg kg^{-1} of ketamine and 10 mg kg^{-1} of xylazine injected i.p. and were then restrained supine, intubated and ventilated with a respirator (Harvard Apparatus). After shaving of the left anterior chest, the intercostal muscles were dissected and aorta identified, then freed by blunt dissection. A 7-0 silk suture was placed around the transverse aorta and tied around a blunt 26-gauge needle. The needle was then removed after placement of the constrictor. Immediately following the first procedure, the LV and left main coronary artery system were exposed and the apical portion of the left anterior descending coronary artery was ligated with 9-0 silk suture. The surgical incision was closed, and the mice were recovered on a warmer until arousal from anaesthesia when they were returned to their home cage. All surgeries were performed in under 20 min. Mice were killed 4 weeks after sham or TAC + MI surgery by CO$_2$ asphyxiation after a 4-h fast for collection of plasma and tissues.

Ketone body injection. Here, 12-week-old CS-MPC2$^{-/-}$ mice underwent echocardiography as detailed above and were then randomized into two groups to receive daily i.p. injections of either saline vehicle or 10 mmol kg^{-1} R-3-hydroxybutyric acid sodium salt (βHB) (Sigma), which had the pH adjusted to roughly 7.0. After 2 weeks of daily i.p. injection, echocardiography was repeated following the same procedures as detailed above. The following day, mice received a final saline or βHB injection, were fasted for 4 h, and were euthanized by CO$_2$ asphyxiation for collection of plasma and tissues.

Cardiac glycogen assay. Glycogen concentrations were measured in a similar fashion as performed previously[79]. Then, 15–60 mg of heart tissue was placed into 2-ml microcentrifuge tubes and boiled in 300 μl of 30% KOH at 100 °C for 30 min, with vortex mixing every 10 min. Tubes were cooled on ice and then 100 μl of 2% Na$_2$SO$_4$ and 800 μl of 100% EtOH was added and tubes vortexed. Tubes were boiled again for 5 min to aid in the precipitation of glycogen and then tubes centrifuged at 16,000g for 5 min and supernatant aspirated. The pellet was dissolved in 1 ml

of 80% EtOH, vortexed and recentrifuged 16,000*g* for 5 min, and this wash was repeated once more (three total pelleting steps). The final pellets were resuspended in 200 µl of 0.3 mg ml^{-1} amyloglucosidase (Sigma) in 0.2 M sodium acetate. Serial dilutions of 10 mg ml^{-1} oyster glycogen (Sigma) were prepared as standards. Samples and standards were then incubated in a 40 °C water bath for 3 h. Samples and standards were then diluted 1:1 with H$_2$O, and 5 µl of each added to a 96-well plate. Next, 200 µl of glucose assay buffer (0.3 M triethanolamine, pH 7.5, 4 mM MgCl$_2$, 2 mM ATP, 0.9 mM NADP$^+$ and 5 µg ml^{-1} of glucose-6-phosphate dehydrogenase, all from Sigma) was then added to each well, and the absorbance at 340 nm measured. Then 1 µg of hexokinase (Sigma) was then added to each well, and the plate incubated at room temperature in the dark for 30 min, then the absorbance again read at 340 nm. The glycogen concentration was calculated from the difference in absorbance readings and plotted in relation to the oyster glycogen standards.

Statistical analysis. All data are presented as dot plots with mean ± s.e.m., or as pre–post data points. All data were first entered into Microsoft Excel v.16.4 and then imported into GraphPad Prism 8.4.2 for graphing and statistical analysis. Multiple comparisons were analysed using a two-way analysis of variance (ANOVA) with Tukey's multiple-comparisons test. An unpaired, two-tailed Student's *t*-test was used for comparison of two groups. A *P* value of less than 0.05 was considered statistically significant.

Reporting Summary. Further information on research design is available in the Nature Research Reporting Summary linked to this article.

Data availability
All data from these studies are contained within this manuscript, the figures, and extended/supplemental figures and tables. Data are also available from the corresponding author upon reasonable request. Source data are provided with this paper.

References
1. Bing, R. J., Siegel, A., Ungar, I. & Gilbert, M. Metabolism of the human heart. II. Studies on fat, ketone and amino acid metabolism. *Am. J. Med.* **16**, 504–515 (1954).
2. Wisneski, J. A., Gertz, E. W., Neese, R. A. & Mayr, M. Myocardial metabolism of free fatty acids. Studies with 14C-labeled substrates in humans. *J. Clin. Invest.* **79**, 359–366 (1987).
3. Lopaschuk, G. D. & Spafford, M. A. Energy substrate utilization by isolated working hearts from newborn rabbits. *Am. J. Physiol.* **258**, H1274–H1280 (1990).
4. Glatz, J. F. & Veerkamp, J. H. Postnatal development of palmitate oxidation and mitochondrial enzyme activities in rat cardiac and skeletal muscle. *Biochim. Biophys. Acta* **711**, 327–335 (1982).
5. Lopaschuk, G. D., Spafford, M. A. & Marsh, D. R. Glycolysis is predominant source of myocardial ATP production immediately after birth. *Am. J. Physiol.* **261**, H1698–H1705 (1991).
6. Kaijser, L. & Berglund, B. Myocardial lactate extraction and release at rest and during heavy exercise in healthy men. *Acta Physiol. Scand.* **144**, 39–45 (1992).
7. Vanoverschelde, J. L. et al. Competition between palmitate and ketone bodies as fuels for the heart: study with positron emission tomography. *Am. J. Physiol.* **264**, H701–H707 (1993).
8. Jeffrey, F. M., Diczku, V., Sherry, A. D. & Malloy, C. R. Substrate selection in the isolated working rat heart: effects of reperfusion, afterload, and concentration. *Basic Res. Cardiol.* **90**, 388–396 (1995).
9. Stanley, W. C., Meadows, S. R., Kivilo, K. M., Roth, B. A. & Lopaschuk, G. D. beta-Hydroxybutyrate inhibits myocardial fatty acid oxidation in vivo independent of changes in malonyl-CoA content. *Am. J. Physiol. Heart Circ. Physiol.* **285**, H1626–H1631 (2003).
10. Garnier, A. et al. Depressed mitochondrial transcription factors and oxidative capacity in rat failing cardiac and skeletal muscles. *J. Physiol.* **551**, 491–501 (2003).
11. Heinke, M. Y. et al. Changes in myocardial protein expression in pacing-induced canine heart failure. *Electrophoresis* **20**, 2086–2093 (1999).
12. Ide, T. et al. Mitochondrial DNA damage and dysfunction associated with oxidative stress in failing hearts after myocardial infarction. *Circ. Res.* **88**, 529–535 (2001).
13. Marin-Garcia, J., Goldenthal, M. J. & Moe, G. W. Abnormal cardiac and skeletal muscle mitochondrial function in pacing-induced cardiac failure. *Cardiovasc. Res.* **52**, 103–110 (2001).
14. Sack, M. N. et al. Fatty acid oxidation enzyme gene expression is downregulated in the failing heart. *Circulation* **94**, 2837–2842 (1996).
15. Warren, J. S., Oka, S. I., Zablocki, D. & Sadoshima, J. Metabolic reprogramming via PPARalpha signaling in cardiac hypertrophy and failure: from metabolomics to epigenetics. *Am. J. Physiol. Heart Circ. Physiol.* **313**, H584–H596 (2017).
16. Barger, P. M., Brandt, J. M., Leone, T. C., Weinheimer, C. J. & Kelly, D. P. Deactivation of peroxisome proliferator-activated receptor-alpha during cardiac hypertrophic growth. *J. Clin. Invest.* **105**, 1723–1730 (2000).
17. Taegtmeyer, H. & Overturf, M. L. Effects of moderate hypertension on cardiac function and metabolism in the rabbit. *Hypertension* **11**, 416–426 (1988).
18. Zhabyeyev, P. et al. Pressure-overload-induced heart failure induces a selective reduction in glucose oxidation at physiological afterload. *Cardiovasc. Res.* **97**, 676–685 (2013).
19. Herzig, S. et al. Identification and functional expression of the mitochondrial pyruvate carrier. *Science* **337**, 93–96 (2012).
20. Bricker, D. K. et al. A mitochondrial pyruvate carrier required for pyruvate uptake in yeast, Drosophila, and humans. *Science* **337**, 96–100 (2012).
21. Chambers, K. T. et al. Chronic inhibition of pyruvate dehydrogenase in heart triggers an adaptive metabolic response. *J. Biol. Chem.* **286**, 11155–11162 (2011).
22. Zhao, G. et al. Overexpression of pyruvate dehydrogenase kinase 4 in heart perturbs metabolism and exacerbates calcineurin-induced cardiomyopathy. *Am. J. Physiol. Heart Circ. Physiol.* **294**, H936–H943 (2008).
23. Gopal, K. et al. Cardiac-specific deletion of pyruvate dehydrogenase impairs glucose oxidation rates and induces diastolic dysfunction. *Front Cardiovasc. Med.* **5**, 17 (2018).
24. Sun, W. et al. Cardiac-specific deletion of the Pdha1 gene sensitizes heart to toxicological actions of ischemic stress. *Toxicol. Sci.* **151**, 193–203 (2016).
25. Sheeran, F. L., Angerosa, J., Liaw, N. Y., Cheung, M. M. & Pepe, S. Adaptations in protein expression and regulated activity of pyruvate dehydrogenase multienzyme complex in human systolic heart failure. *Oxid. Med. Cell Longev.* **2019**, 4532592 (2019).
26. McCommis, K. S. et al. Loss of mitochondrial pyruvate carrier 2 in the liver leads to defects in gluconeogenesis and compensation via pyruvate-alanine cycling. *Cell Metab.* **22**, 682–694 (2015).
27. McCommis, K. S. et al. An ancestral role for the mitochondrial pyruvate carrier in glucose-stimulated insulin secretion. *Mol. Metab.* **5**, 602–614 (2016).
28. McCommis, K. S. et al. Targeting the mitochondrial pyruvate carrier attenuates fibrosis in a mouse model of nonalcoholic steatohepatitis. *Hepatology* **65**, 1543–1556 (2017).
29. Chen, J., Kubalak, S. W. & Chien, K. R. Ventricular muscle-restricted targeting of the RXRalpha gene reveals a non-cell-autonomous requirement in cardiac chamber morphogenesis. *Development* **125**, 1943–1949 (1998).
30. Halestrap, A. P. & Denton, R. M. The specificity and metabolic implications of the inhibition of pyruvate transport in isolated mitochondria and intact tissue preparations by alpha-Cyano-4-hydroxycinnamate and related compounds. *Biochem. J.* **148**, 97–106 (1975).
31. Aubert, G. et al. The failing heart relies on ketone bodies as a fuel. *Circulation* **133**, 698–705 (2016).
32. Bedi, K. C. Jr. et al. Evidence for intramyocardial disruption of lipid metabolism and increased myocardial ketone utilization in advanced human heart failure. *Circulation* **133**, 706–716 (2016).
33. Horton, J. L. et al. The failing heart utilizes 3-hydroxybutyrate as a metabolic stress defense. *JCI Insight* **4**, e124079 (2019).
34. Sciarretta, S., Forte, M., Frati, G. & Sadoshima, J. New insights into the role of mTOR signaling in the cardiovascular system. *Circ. Res.* **122**, 489–505 (2018).
35. Wentz, A. E. et al. Adaptation of myocardial substrate metabolism to a ketogenic nutrient environment. *J. Biol. Chem.* **285**, 24447–24456 (2010).
36. Ford, D. A., Han, X., Horner, C. C. & Gross, R. W. Accumulation of unsaturated acylcarnitine molecular species during acute myocardial ischemia: metabolic compartmentalization of products of fatty acyl chain elongation in the acylcarnitine pool. *Biochemistry* **35**, 7903–7909 (1996).
37. Martin, M. A. et al. Myocardial carnitine and carnitine palmitoyltransferase deficiencies in patients with severe heart failure. *Biochim. Biophys. Acta* **1502**, 330–336 (2000).
38. Stanley, W. C., Recchia, F. A. & Lopaschuk, G. D. Myocardial substrate metabolism in the normal and failing heart. *Physiol. Rev.* **85**, 1093–1129 (2005).
39. Shearman, M. S. & Halestrap, A. P. The concentration of the mitochondrial pyruvate carrier in rat liver and heart mitochondria determined with alpha-cyano-beta-(1-phenylindol-3-yl)acrylate. *Biochem. J.* **223**, 673–676 (1984).
40. Hildyard, J. C., Ammala, C., Dukes, I. D., Thomson, S. A. & Halestrap, A. P. Identification and characterisation of a new class of highly specific and potent inhibitors of the mitochondrial pyruvate carrier. *Biochim. Biophys. Acta* **1707**, 221–230 (2005).

41. Bunger, R. & Mallet, R. T. Mitochondrial pyruvate transport in working guinea-pig heart. Work-related vs. carrier-mediated control of pyruvate oxidation. *Biochim. Biophys. Acta* **1151**, 223–236 (1993).

42. Fernandez-Caggiano, M. et al. Analysis of mitochondrial proteins in the surviving myocardium after ischemia identifies mitochondrial pyruvate carrier expression as possible mediator of tissue viability. *Mol. Cell Proteom.* **15**, 246–255 (2016).

43. Fernandez-Caggiano, M. et al. Mitochondrial pyruvate carrier abundance mediates pathological cardiac hypertrophy. *Nat. Metabol.* https://doi.org/10.1038/s42255-020-00276-5 (2020).

44. Zhang, Y. et al. Mitochondrial pyruvate carriers are required for myocardial stress adaptation. *Nat. Metabol.* https://doi.org/10.1038/s42255-020-00288-1 (2020).

45. Malloy, C. R., Sherry, A. D. & Jeffrey, F. M. Evaluation of carbon flux and substrate selection through alternate pathways involving the citric acid cycle of the heart by 13C NMR spectroscopy. *J. Biol. Chem.* **263**, 6964–6971 (1988).

46. Sundqvist, K. E., Hiltunen, J. K. & Hassinen, I. E. Pyruvate carboxylation in the rat heart. Role of biotin-dependent enzymes. *Biochem J.* **257**, 913–916 (1989).

47. Karlstaedt, A. et al. Oncometabolite d-2-hydroxyglutarate impairs alpha-ketoglutarate dehydrogenase and contractile function in rodent heart. *Proc. Natl Acad. Sci. USA* **113**, 10436–10441 (2016).

48. Akbay, E. A. et al. D-2-hydroxyglutarate produced by mutant IDH2 causes cardiomyopathy and neurodegeneration in mice. *Genes Dev.* **28**, 479–490 (2014).

49. Karlstaedt, A., Khanna, R., Thangam, M. & Taegtmeyer, H. Glucose 6-phosphate accumulates via phosphoglucose isomerase inhibition in heart muscle. *Circ. Res.* **126**, 60–74 (2020).

50. Ritterhoff, J. et al. Metabolic remodeling promotes cardiac hypertrophy by directing glucose to aspartate biosynthesis. *Circ. Res.* **126**, 182–196 (2020).

51. Sung, M. M. et al. AMPK deficiency in cardiac muscle results in dilated cardiomyopathy in the absence of changes in energy metabolism. *Cardiovasc. Res.* **107**, 235–245 (2015).

52. Xing, Y. et al. Glucose metabolism and energy homeostasis in mouse hearts overexpressing dominant negative alpha2 subunit of AMP-activated protein kinase. *J. Biol. Chem.* **278**, 28372–28377 (2003).

53. Zarrinpashneh, E. et al. AMPKalpha2 counteracts the development of cardiac hypertrophy induced by isoproterenol. *Biochem. Biophys. Res. Commun.* **376**, 677–681 (2008).

54. Kim, M. et al. Mutation in the gamma2-subunit of AMP-activated protein kinase stimulates cardiomyocyte proliferation and hypertrophy independent of glycogen storage. *Circ. Res.* **114**, 966–975 (2014).

55. Nielsen, R. et al. Cardiovascular effects of treatment with the ketone body 3-hydroxybutyrate in chronic heart failure patients. *Circulation* **139**, 2129–2141 (2019).

56. Uchihashi, M. et al. Cardiac-specific Bdh1 overexpression ameliorates oxidative stress and cardiac remodeling in pressure overload-induced heart failure. *Circ. Heart. Fail.* **10**, e004417 (2017).

57. Schugar, R. C. et al. Cardiomyocyte-specific deficiency of ketone body metabolism promotes accelerated pathological remodeling. *Mol. Metab.* **3**, 754–769 (2014).

58. Pereyra, A. S. et al. Loss of cardiac carnitine palmitoyltransferase 2 results in rapamycin-resistant, acetylation-independent hypertrophy. *J. Biol. Chem.* **292**, 18443–18456 (2017).

59. Halestrap, A. P. Pyruvate and ketone-body transport across the mitochondrial membrane. Exchange properties, pH-dependence and mechanism of the carrier. *Biochem. J.* **172**, 377–387 (1978).

60. Gray, L. R. et al. Hepatic mitochondrial pyruvate carrier 1 is required for efficient regulation of gluconeogenesis and whole-body glucose homeostasis. *Cell Metab.* **22**, 669–681 (2015).

61. National Institutes of Health. *Guide for the Care and Use of Laboratory Animals* (National Academies Press, 2011).

62. Chen, J. et al. Selective requirement of myosin light chain 2v in embryonic heart function. *J. Biol. Chem.* **273**, 1252–1256 (1998).

63. Vigueira, P. A. et al. Mitochondrial pyruvate carrier 2 hypomorphism in mice leads to defects in glucose-stimulated insulin secretion. *Cell Rep.* **7**, 2042–2053 (2014).

64. Bowman, C. E., Zhao, L., Hartung, T. & Wolfgang, M. J. Requirement for the mitochondrial pyruvate carrier in mammalian development revealed by a hypomorphic allelic series. *Mol. Cell. Biol.* **36**, 2089–2104 (2016).

65. Exil, V. J. et al. Very-long-chain acyl-coenzyme a dehydrogenase deficiency in mice. *Circ. Res.* **93**, 448–455 (2003).

66. Hainline, B. E., Kahlenbeck, D. J., Grant, J. & Strauss, A. W. Tissue specific and developmental expression of rat long-and medium-chain acyl-CoA dehydrogenases. *Biochim. Biophys. Acta* **1216**, 460–468 (1993).

67. Kelly, D. P. et al. Nucleotide sequence of medium-chain acyl-CoA dehydrogenase mRNA and its expression in enzyme-deficient human tissue. *Proc. Natl Acad. Sci. USA* **84**, 4068–4072 (1987).

68. An, J. et al. Hepatic expression of malonyl-CoA decarboxylase reverses muscle, liver and whole-animal insulin resistance. *Nat. Med.* **10**, 268–274 (2004).

69. Ferrara, C. T. et al. Genetic networks of liver metabolism revealed by integration of metabolic and transcriptional profiling. *PLoS Genet.* **4**, e1000034 (2008).

70. Millington, D. S. & Stevens, R. D. Acylcarnitines: analysis in plasma and whole blood using tandem mass spectrometry. *Methods Mol. Biol.* **708**, 55–72 (2011).

71. Chace, D. H. et al. Rapid diagnosis of phenylketonuria by quantitative analysis for phenylalanine and tyrosine in neonatal blood spots by tandem mass spectrometry. *Clin. Chem.* **39**, 66–71 (1993).

72. Jensen, M. V. et al. Compensatory responses to pyruvate carboxylase suppression in islet beta-cells. Preservation of glucose-stimulated insulin secretion. *J. Biol. Chem.* **281**, 22342–22351 (2006).

73. Khomtchouk, B. B., Hennessy, J. R. & Wahlestedt, C. shinyheatmap: Ultra fast low memory heatmap web interface for big data genomics. *PLoS One* **12**, e0176334 (2017).

74. Gao, L. et al. Simultaneous quantification of malonyl-CoA and several other short-chain acyl-CoAs in animal tissues by ion-pairing reversed-phase HPLC/MS. *J. Chromatogr. B. Anal. Technol. Biomed. Life Sci.* **853**, 303–313 (2007).

75. Weinheimer, C. J., Lai, L., Kelly, D. P. & Kovacs, A. Novel mouse model of left ventricular pressure overload and infarction causing predictable remodelling and progression to heart failure. *Clin. Exp. Pharm. Physiol.* **42**, 33–40 (2015).

76. Teichholz, L. E., Kreulen, T., Herman, M. V. & Gorlin, R. Problems in echocardiographic volume determinations: echocardiographic-angiographic correlations in the presence of absence of asynergy. *Am. J. Cardiol.* **37**, 7–11 (1976).

77. Kronik, G., Slany, J. & Mosslacher, H. Comparative value of eight M-mode echocardiographic formulas for determining left ventricular stroke volume. A correlative study with thermodilution and left ventricular single-plane cineangiography. *Circulation* **60**, 1308–1316 (1979).

78. Weinheimer, C. J. et al. Load-dependent changes in left ventricular structure and function in a pathophysiologically relevant murine model of reversible heart failure. *Circ. Heart Fail.* **11**, e004351 (2018).

79. Suzuki, Y. et al. Insulin control of glycogen metabolism in knockout mice lacking the muscle-specific protein phosphatase PP1G/RGL. *Mol. Cell. Biol.* **21**, 2683–2694 (2001).

Acknowledgements

Author contributions

K.S.M. and B.N.F. conceived the study. K.S.M., A.K., C.J.W., T.M.S., T.R.K., O.R.I., D.M.M. and B.N.F. designed the study. Acquisition and analysis were conducted by K.S.M., A.K., C.J.W., T.R.K., O.R.I., D.R.K. and K.D.P. The resources were obtained by M.T.K., R.L.V., B.J.D. and R.W.G. Writing and editing of the manuscript were done by K.S.M., A.K., C.J.W., T.M.S., T.R.K., O.R.I., D.M.M., D.R.K., K.D.P., M.T.K., B.J.D., R.W.G. and B.N.F.

Competing interests

Additional information
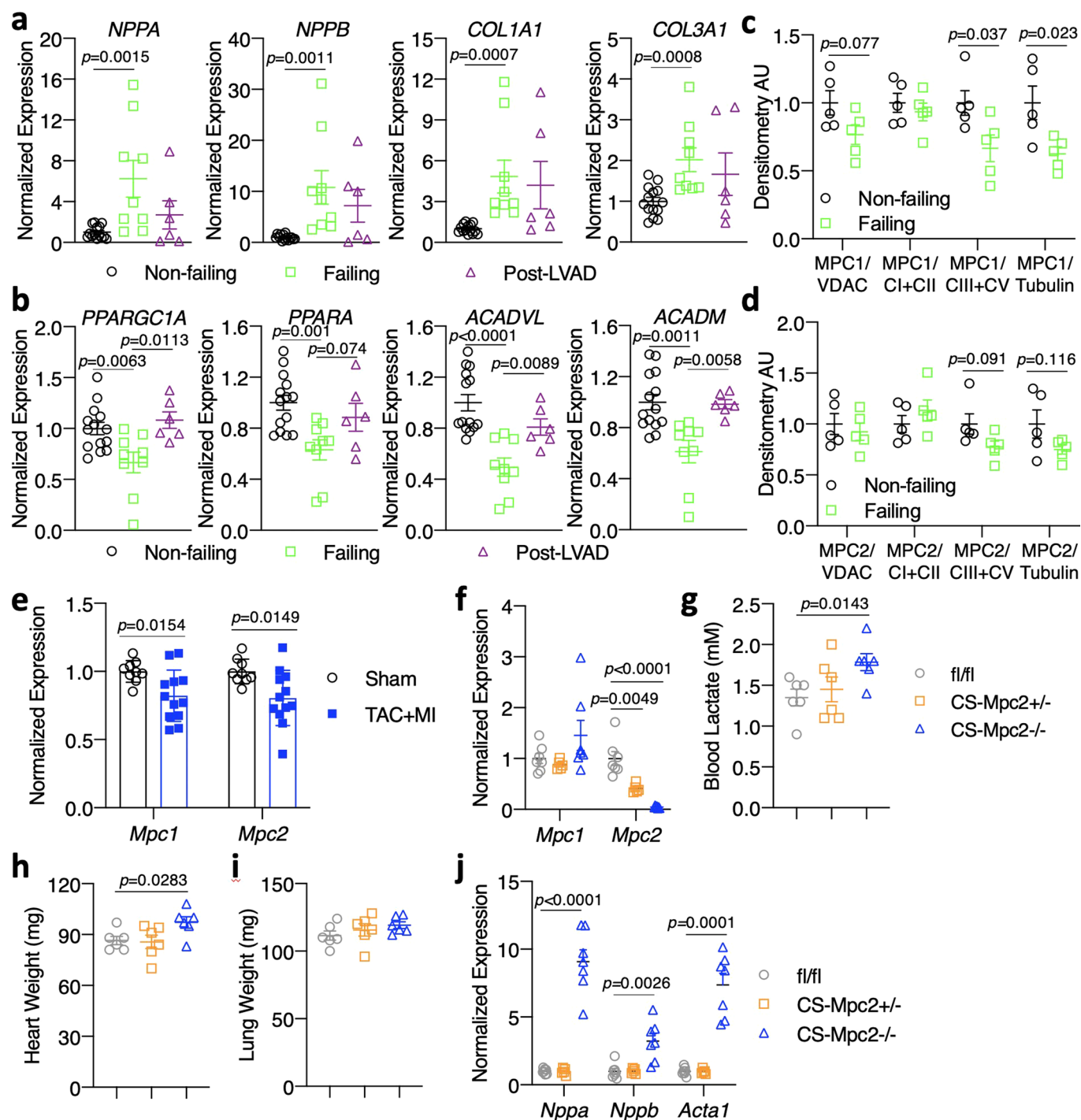
Extended Data Fig. 1 | Human heart failure gene expression and characterization of 6-week old CS-MPC2−/− mice. Gene expression from human non-failing, failing, and failing hearts after left ventricular assist device (LVAD) placement (n=14, 9, and 6 for Non-failing, Failing, and Post-LVAD, respectively). **c-d**, MPC1 and MPC2 protein expression quantification from non-failing and failing human hearts normalized to either VDAC, complex I and II, complexes III and IV, or Tubulin (n=5). **e**, Gene expression for *Mpc1* and *Mpc2* from wildtype C57BL6/J mouse hearts after sham or transverse aortic constriction plus myocardial infarction (TAC + MI) surgery (n=9 sham, 12 TAC-MI). **f**, Mouse heart gene expression for *Mpc1* and *Mpc2* (n=7, 5, 7 for fl/fl, +/−, −/− respectively). **g**, Blood lactate measured after a 4h fast prior to sacrifice in 6-week old mice (n=6). **h-i**, Heart weight and lung weight of 6-week old mice (n=6). **j**, Mouse heart gene expression of heart failure, and hypertrophy genes from 6-week old mice (n=7, 5, 7 for fl/fl, +/−, −/− respectively). Data are presented as mean ± s.e.m. within dot plot. Each data point represents one individual mouse or sample. Two-tailed unpaired Student's *t* test.
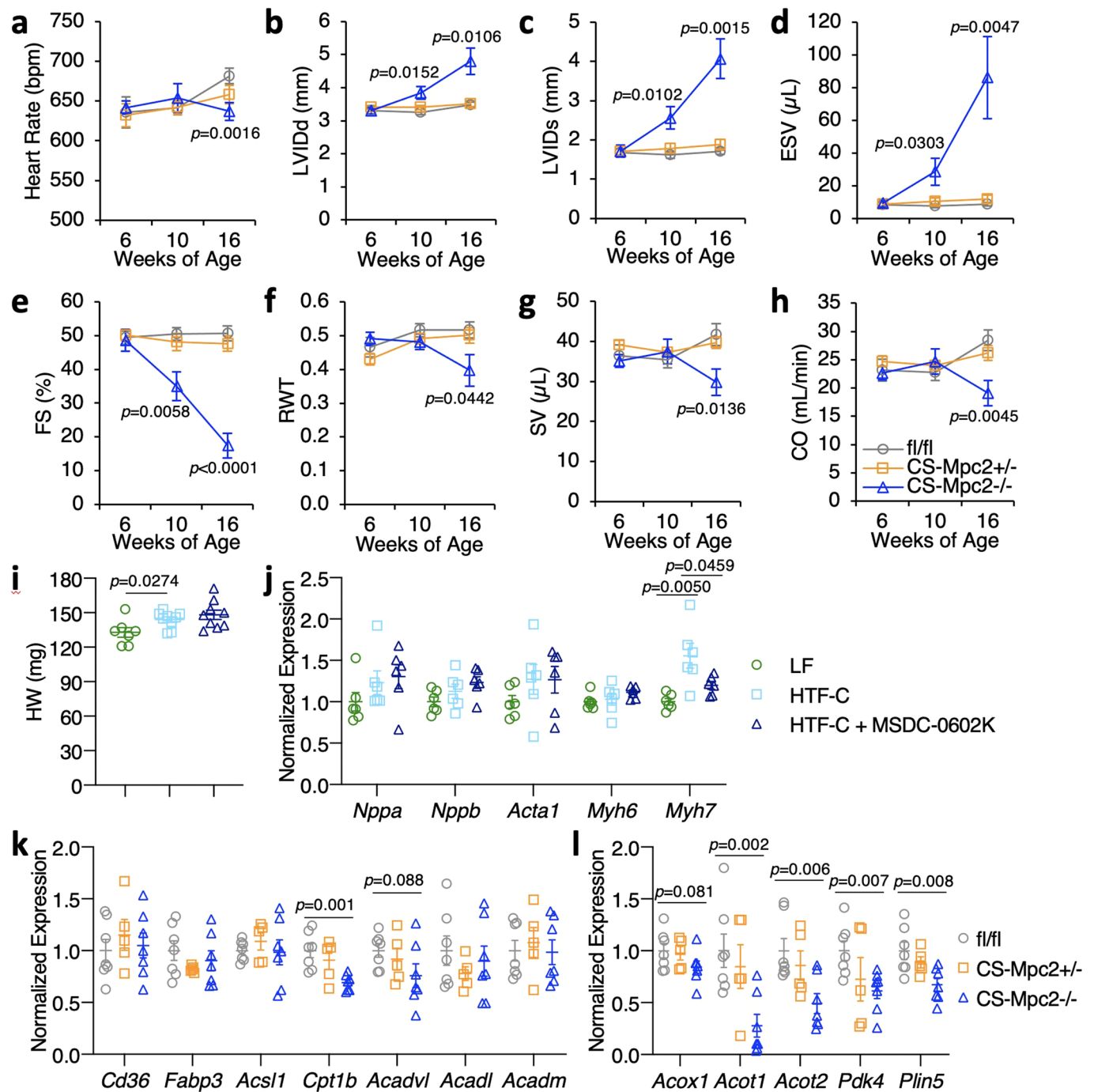
Extended Data Fig. 2 | Heart failure develops in CS-MPC2−/− mice, but not CS-MPC2 +/− or mice treated with the MPC inhibitor MSDC-0602K. a-h, Serial echocardiography data of chow-fed mice at 6, 10, and 16 weeks of age. Left ventricular internal diameter at end diastole (LVIDd) and end systole (LVIDs), end systolic volume (ESV), fractional shortening (FS), relative wall thickness (RWT), stroke volume (SV), and cardiac output (CO) (n = 7, 10, and 9 for fl/fl, +/−, and −/−, respectively). **i,** Heart weights from WT mice fed low fat (LF) diet or a high trans-fat, fructose, cholesterol (HTF-C) diet +/− 330 ppm MSDC-0602, an insulin-sensitizing MPC inhibitor (n = 7, 9, and 9 for LF, HTF-C, and HTF-C + MSDC-0602K, respectively). **j,** Heart gene expression of hypertrophy gene markers from WT mice fed LF, HTF-C, or HTF-C + MSDC-0602 diets (n = 6 for all groups). **k-l,** Heart gene expression for fatty acid transport and oxidation genes and PPARα target genes from chow-fed 16-week old mice after a 4 h fast (n = 7, 5, and 7 for fl/fl, +/−, and −/−, respectively). Data are presented as mean ± s.e.m., or mean ± s.e.m. within dot plot. Each data point represents one individual mouse or sample. Two-tailed unpaired Student's t test.
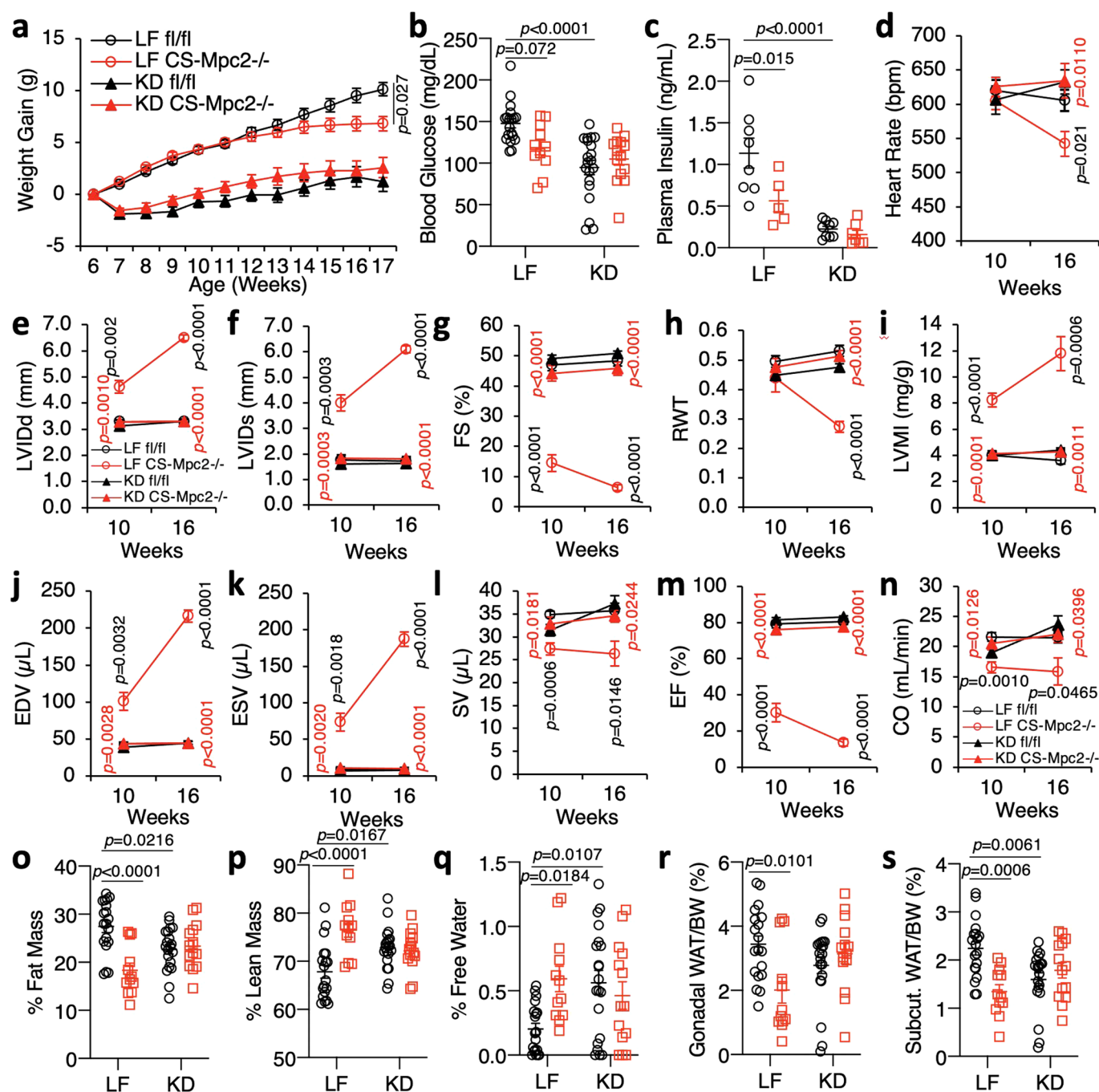
Extended Data Fig. 3 | Ketogenic diet prevents heart failure in CS-MPC2−/− mice. a, Body weights of mice fed low fat (LF) or ketogenic diet (KD) from 6-17 weeks of age (initial n = 19, 15, 21, and 14 for fl/fl LF, CS-Mpc2−/− LF, fl/fl KD, and CS-Mpc2−/− KD, respectively)(fl/fl LF vs KD $p < 0.0001$; CS-Mpc2−/− LF vs KD $p < 0.0001$). **b-c**, Blood glucose and plasma insulin measured after a 4 h fast (n = 19, 11, 20, and 14, respectively for glucose and 8, 5, 9, and 7, respectively for insulin). **d-n**, Echocardiography data at 10 and 16 weeks of age. Left ventricular internal diameter at end diastole (LVIDd) and end systole (LVIDs), fractional shortening (FS), relative wall thickness (RWT), end diastolic volume (EDV), end systolic volume (ESV), stroke volume (SV), ejection fraction (EF), and cardiac output (CO) (n = 9, 7, 12, and 9 for fl/fl LF, CS-Mpc2−/− LF, fl/fl KD, and CS-Mpc2−/− KD, respectively). **o-q**, % Fat mass, % lean mass, and % free water body composition measured by echoMRI (n = 19, 12, 20, and 14, respectively). **r-s**, Gonadal and inguinal white adipose tissue (WAT) weights normalized to body weight (n = 19, 12, 20, and 14, respectively). Data are presented as mean ± s.e.m. or mean ± s.e.m. within dot plot. Each data point in dot plot represents one individual mouse sample. Two-way ANOVA with Tukey's multiple comparisons test. For **d-n**, black p values indicate LF-fed fl/fl vs. CS-Mpc2−/−, red p values indicate LF vs. KD for CS-Mpc2−/− for each echocardiography date.
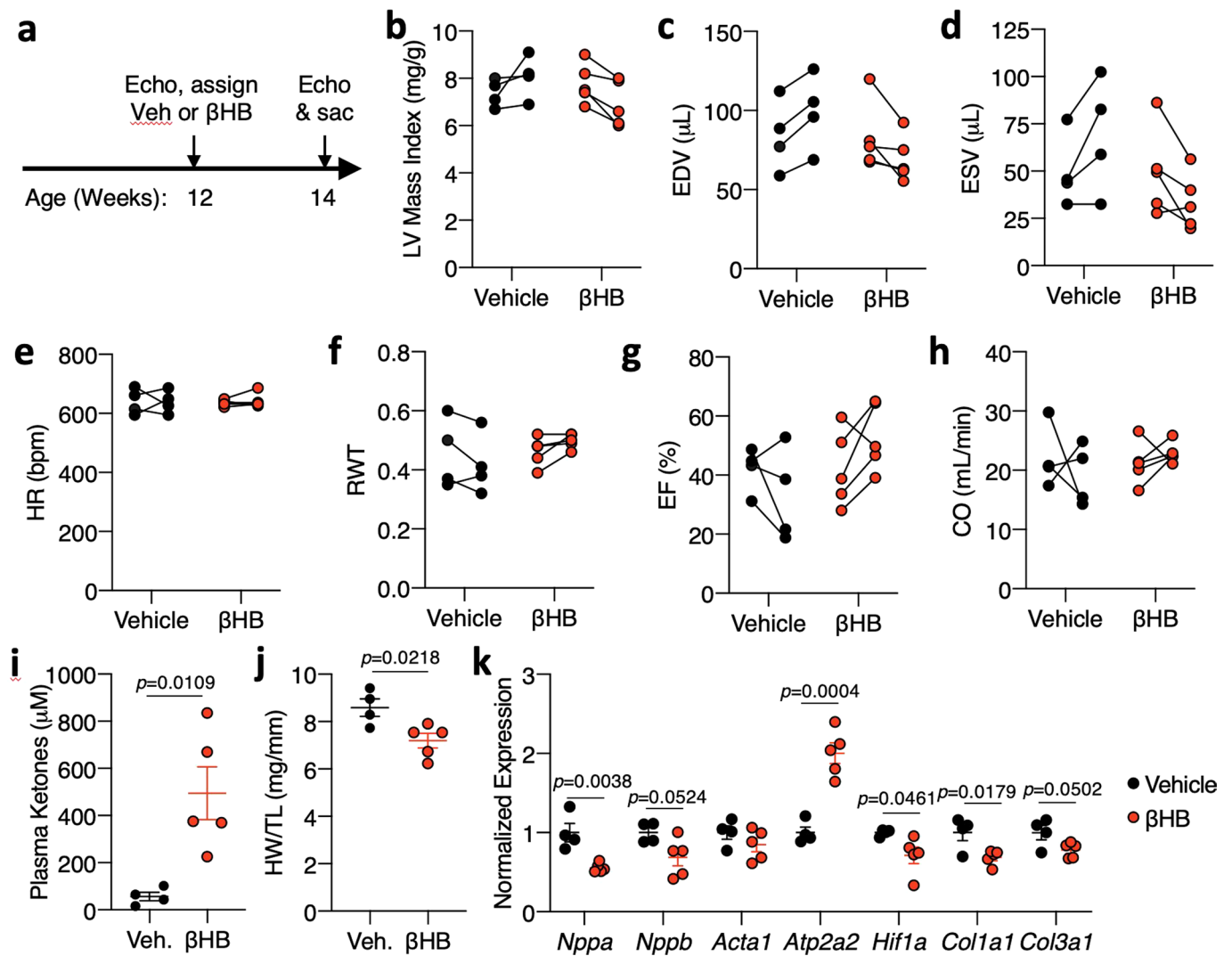
Extended Data Fig. 4 | Ketone body injection modestly reduces cardiac remodeling in CS-MPC2−/− mice. a, Timeline for β-hydroxybutyrate (βHB) injection experiment in which CS-MPC2−/− mice were injected i.p. with saline vehicle or 10 mmol/kg βHB daily from 12 to 14 weeks of age. **b-h**, Echocardiography measurements before and after 2 weeks of daily i.p. injection of saline vehicle (Veh) or 10 mmol/kg β-hydroxybutyrate. Left ventricular (LV) mass index, end-diastolic volume (EDV), end-systolic volume (ESV), heart rate (HR), relative wall thickness (RWT), ejection fraction (EF), and cardiac output (CO) (n = 4 Veh, 5 βHB). **i**, Plasma total ketone body concentrations (n = 4 Veh, 5 βHB). **j**, Heart weight normalized to tibia length (n = 4 Veh, 5 βHB). **k**, Gene expression markers of hypertrophy, heart failure, and fibrosis from hearts after 2 weeks of daily vehicle or βHB treatment (n = 4 Veh, 5 βHB). Data presented either as PRE-POST, or mean ± s.e.m. shown within dot plot. Each symbol represents an individual sample. Two-tailed unpaired Student's *t* test.
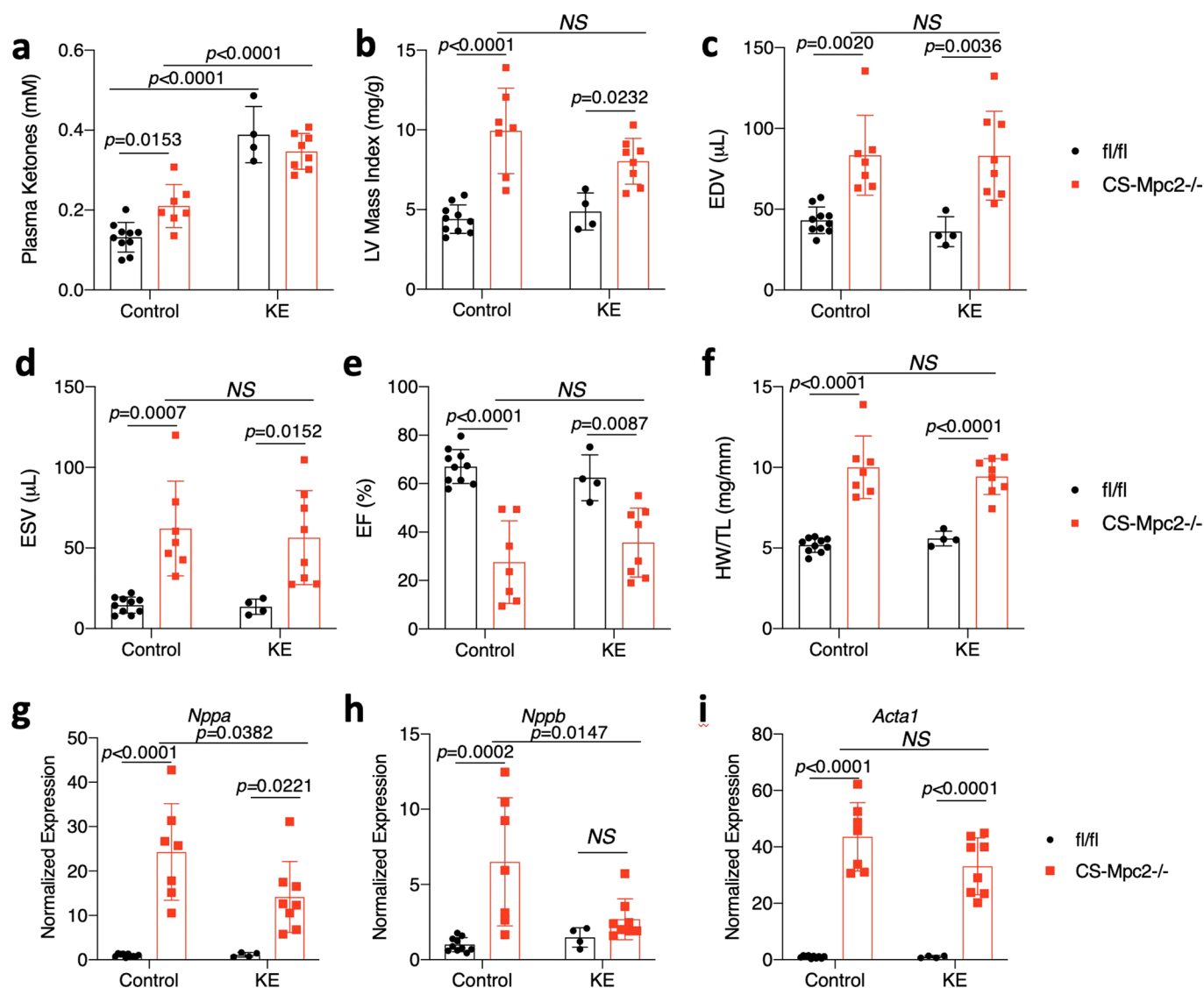
Extended Data Fig. 5 | Ketone ester diet does not improve cardiac remodeling or function in CS-MPC2−/− mice. a, Plasma ketone bodies measured from mice fed either control or ketone ester (KE)-supplemented diet (n = 10, 7, 4, and 8, respectively). **b-e**, Echocardiography measurements after 6 weeks of KE diet feeding. Left ventricular (LV) mass index, end-diastolic volume (EDV), end-systolic volume (ESV), and ejection fraction (EF) (n = 10, 7, 4, and 8, respectively). **f**, Heart weight normalized to tibia length (n = 10, 7, 4, and 8, respectively). **g-i**, Cardiac gene expression markers of hypertrophy and heart failure (*Nppa*, *Nppb*, *Acta1*) (n = 10, 7, 4, and 8, respectively). Data presented as mean ± s.e.m. shown within dot plot. Each symbol represents an individual sample. Two-way ANOVA with Tukey's multiple comparisons test.
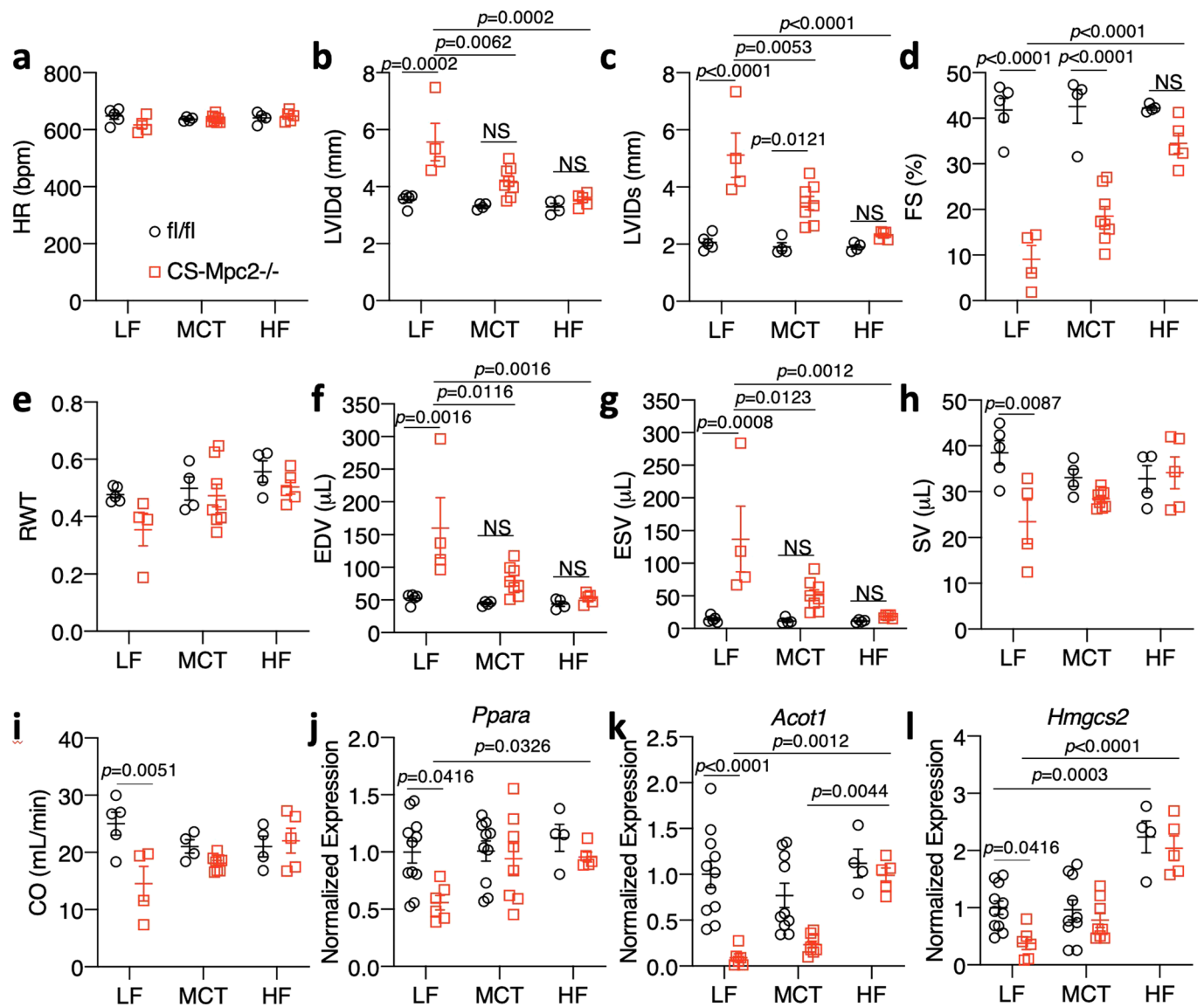
Extended Data Fig. 6 | High-fat diets also greatly improve cardiac remodeling and function of CS-MPC2−/− mice. a-I, Echocardiography measurements taken at 16 weeks of age after 10 weeks of low fat (LF), medium chain triglyceride (MCT), or high-fat (HF) feeding. Left ventricular internal diameter at end diastole (LVIDd) and end systole (LVIDs), fractional shortening (FS), relative wall thickness (RWT), end diastolic volume (EDV), end systolic volume (ESV), stroke volume (SV), and cardiac output (CO) (n = 5, 4, 4, 8, 4, and 5, respectively). **j-l,** Cardiac gene expression for *Ppara* and it's targets *Acot1* and *Hmgcs2* (n = 11, 6, 10, 8, 4, and 5, respectively). Data are presented as mean ± s.e.m. within dot plot. Each data point represents an individual mouse. Two-way ANOVA with Tukey's multiple comparisons test.
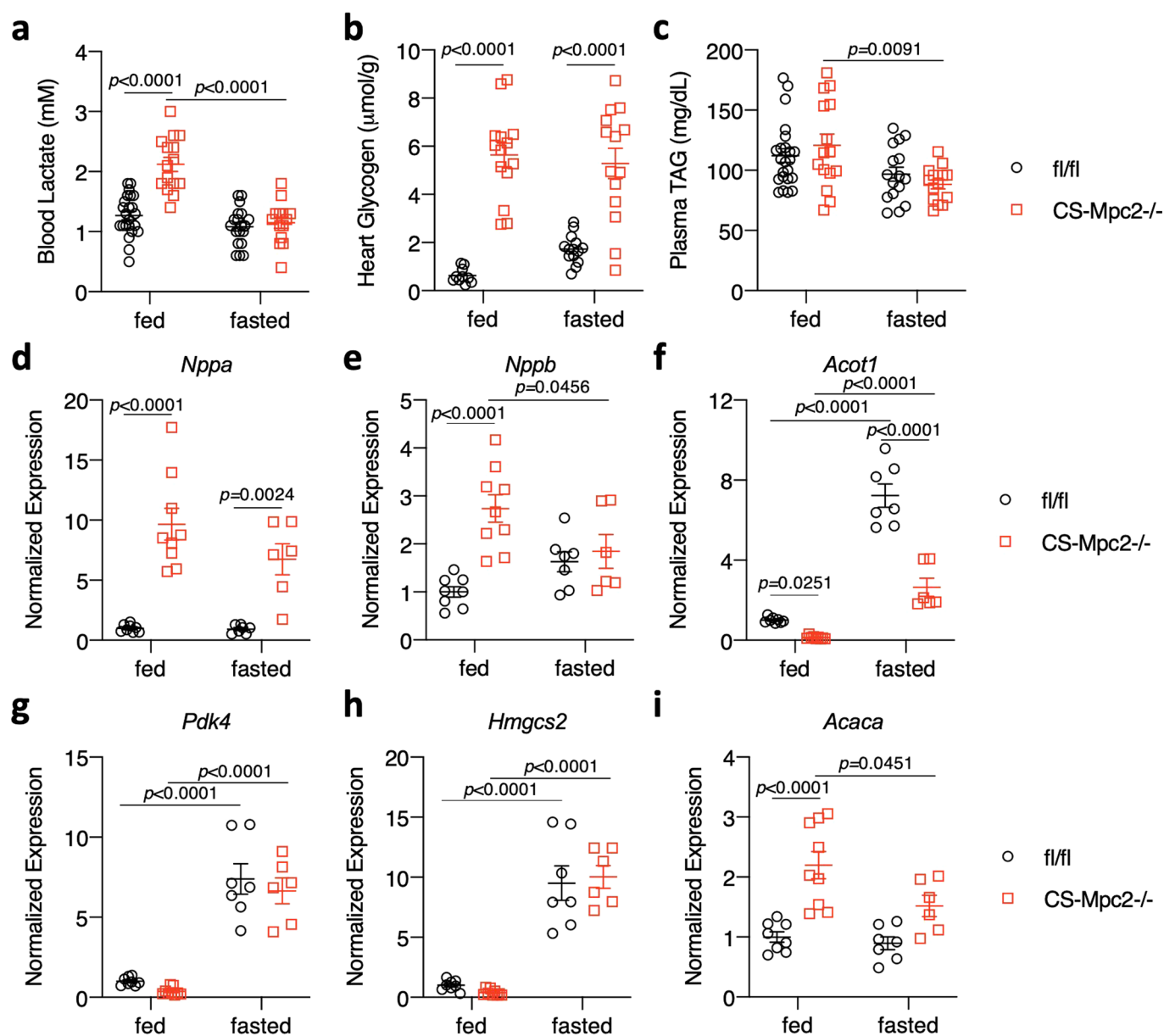
Extended Data Fig. 7 | A 24 hour fast improves cardiac remodeling by enhancing fat oxidation. a, Blood lactate of fed or fasted mice just prior to euthanasia (n = 22, 15, 16, and 14, respectively). **b**, Cardiac glycogen concentrations in hearts of fed and fasted mice (n = 10, 14, 15, and 14, respectively). **c**, Plasma TAG from fed or fasted mice (n = 22, 15, 16, and 14, respectively). **d-i**, Cardiac gene expression for natriuretic peptides and PPARα-target and fatty acid metabolism genes (n = 8, 9, 7, and 6, respectively). Data are presented as mean ± s.e.m. within dot plot. Each symbol on dot plot represents an individual sample. Two-way ANOVA with Tukey's multiple comparisons test.
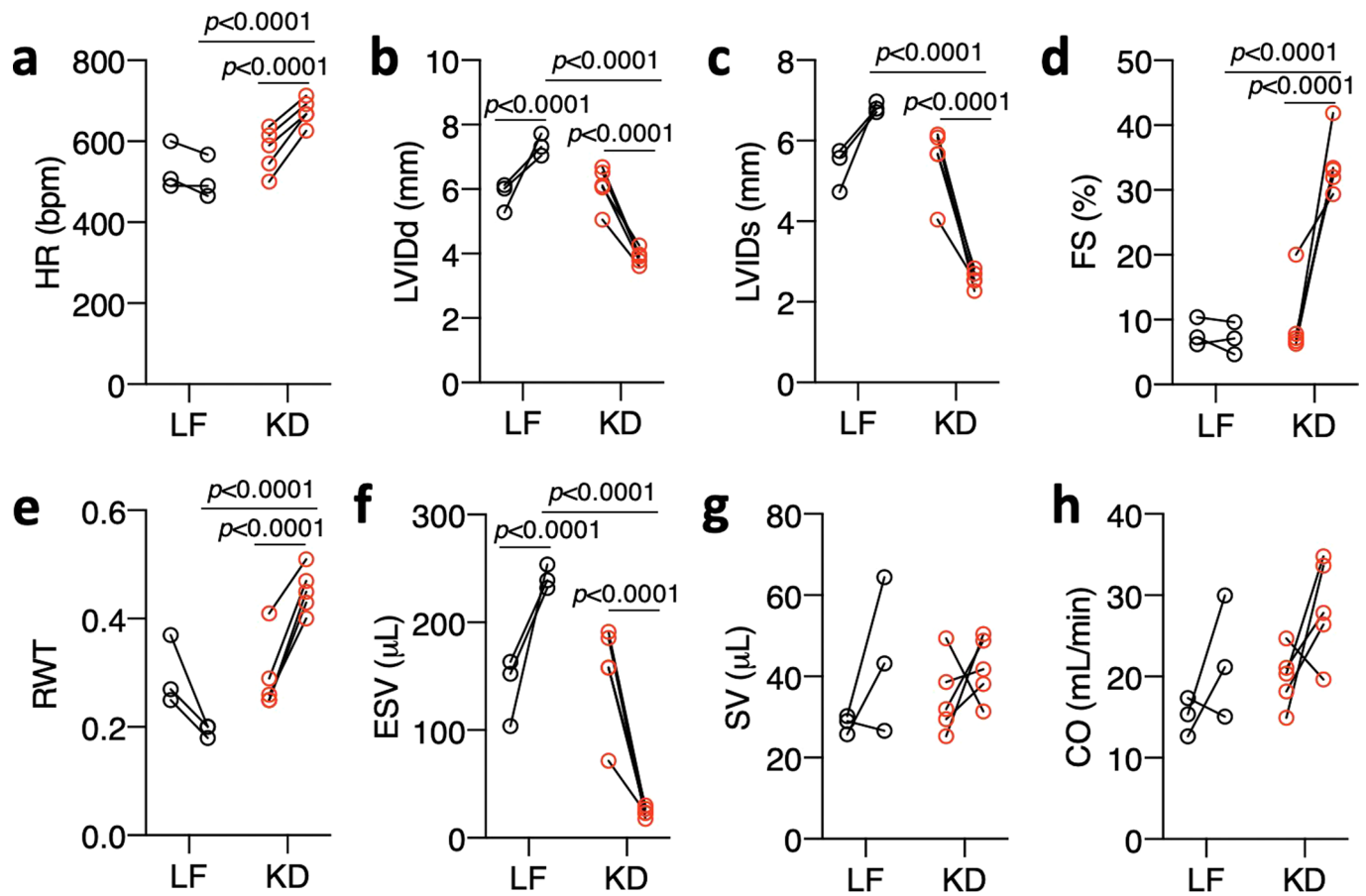
Extended Data Fig. 8 | Ketogenic diet reverses heart failure in CS-MPC2−/− mice. a-h, Echocardiography measurements before and after 3 weeks of LF or KD feeding in 16-week-old CS-MPC2−/− mice with established heart failure (n=3 LF, 5 KD). Data are presented as PRE-POST. Each data point represents an individual mouse. Paired two-tailed student's *t*-test for PRE vs. POST. Unpaired two-tailed student's *t*-test for LF vs. KD.

nature research

Corresponding author(s): Kyle S. McCommis

Last updated by author(s): Sep 7, 2020

Reporting Summary

Nature Research wishes to improve the reproducibility of the work that we publish. This form provides structure for consistency and transparency in reporting. For further information on Nature Research policies, see our Editorial Policies and the Editorial Policy Checklist.

Statistics

For all statistical analyses, confirm that the following items are present in the figure legend, table legend, main text, or Methods section.

n/a	Confirmed	
☐	☒	The exact sample size (*n*) for each experimental group/condition, given as a discrete number and unit of measurement
☐	☒	A statement on whether measurements were taken from distinct samples or whether the same sample was measured repeatedly
☐	☒	The statistical test(s) used AND whether they are one- or two-sided *Only common tests should be described solely by name; describe more complex techniques in the Methods section.*
☐	☒	A description of all covariates tested
☐	☒	A description of any assumptions or corrections, such as tests of normality and adjustment for multiple comparisons
☐	☒	A full description of the statistical parameters including central tendency (e.g. means) or other basic estimates (e.g. regression coefficient) AND variation (e.g. standard deviation) or associated estimates of uncertainty (e.g. confidence intervals)
☐	☒	For null hypothesis testing, the test statistic (e.g. *F*, *t*, *r*) with confidence intervals, effect sizes, degrees of freedom and *P* value noted *Give P values as exact values whenever suitable.*
☒	☐	For Bayesian analysis, information on the choice of priors and Markov chain Monte Carlo settings
☒	☐	For hierarchical and complex designs, identification of the appropriate level for tests and full reporting of outcomes
☒	☐	Estimates of effect sizes (e.g. Cohen's *d*, Pearson's *r*), indicating how they were calculated

Our web collection on statistics for biologists contains articles on many of the points above.

Software and code

Policy information about availability of computer code

Data collection	No custom code was used in data collection. Western blots were imaged and analyzed with ImageStudio and ImageStudio Lite software v5.2.5 from Li-Cor Biosciences. Oxygen consumption rates were measured with DatLab software v7.4 from Oroboros Instruments. The BioTek Synergy plate reader uses Gen5 software. Mouse echocardiography acquisition used Vevo LAB software from VisualSonics Inc.
Data analysis	Heart histology images were analyzed and saved with NIH Image J software v2.0.0. All primary data was entered into Microsoft Excel (v16.4), then data imported into GraphPad Prism (v8.4.2) software for graphing and statistical analyses.

For manuscripts utilizing custom algorithms or software that are central to the research but not yet described in published literature, software must be made available to editors and reviewers. We strongly encourage code deposition in a community repository (e.g. GitHub). See the Nature Research guidelines for submitting code & software for further information.

Data

Policy information about availability of data

All manuscripts must include a data availability statement. This statement should provide the following information, where applicable:

- Accession codes, unique identifiers, or web links for publicly available datasets
- A list of figures that have associated raw data
- A description of any restrictions on data availability

All data associated with these studies are contained within this manuscript, associated data figures, and extended/supplemental figures and tables. Data and resources associated with this manuscript will be shared upon reasonable request to kyle.mccommis@health.slu.edu.

Field-specific reporting

Please select the one below that is the best fit for your research. If you are not sure, read the appropriate sections before making your selection.

☒ Life sciences   ☐ Behavioural & social sciences   ☐ Ecological, evolutionary & environmental sciences

For a reference copy of the document with all sections, see nature.com/documents/nr-reporting-summary-flat.pdf

Life sciences study design

All studies must disclose on these points even when the disclosure is negative.

Sample size	Sample sizes were predicted based on small pilot experiments and extent of phenotype. All experiments were performed with at least 3 smaller cohorts of litter-mate mice and combined.
Data exclusions	No data was excluded from these studies.
Replication	Due to the nature of mouse breeding and births of small litter-mate groups occurring at offset times, essentially all of these in vivo studies were performed with small cohorts of litter-mate mice and then ultimately combined. For the study of chow-fed mice up to 16 weeks of age (Figure 2), four independent cohorts of litter-mate mice were used and similar results replicated each time. For the ketogenic diet study (Figures 3-5), seven independent cohorts of litter-mate mice were used with similar results replicated each time. For the MCT/HFD experiment (Figure 6), four independent cohorts of litter-mate mice were performed with similar results replicated each time. For the fed/ fasting studies, a maximum of 4 mice were used daily (generally 1 for each genotype and fed/fasted condition), and data were obtained from 13 of these small cohorts of litter-mate mice. Heart respiration studies were only performed on 9 of these small cohorts. Similar data was reproduced from each of these small cohorts. Lastly, the ketogenic diet reversal of heart failure study (Figure 8) used a total of 5 independent cohorts of litter-mate mice, sometimes consisting of only a single mouse switching to one of the dietary interventions. As shown in the figures, similar data was obtained from all mice with regards to changes PRE vs POST dietary changes.
Randomization	Of course randomization could not occur for determining WT vs KO mice, nor for the number of mice born in each litter. For all diet studies, the initial cohorts of litter-mate mice were randomly chosen receive either one of each particular diet. The final small cohorts of litter-mate mice were assigned diets based on making sure that each genotype contained a roughly balanced number for each diet, and that all genotype/treatment groups had a roughly balanced number of males/females. Male/female sex of mice was the only covariate taken into account for these studies, and all groups contained a roughly balanced number of male/female mice. Studies of each cohort of mice were timed to start at specific mouse ages, therefore age was not a variable considered in these studies. Lastly, other covariables such as body weight and body composition were not considered when randomizing to treatment group.
Blinding	All echocardiography imaging and analysis was performed by an ultrasonographer that was blinded to mouse genotype. Targeted metabolomics measurement and analysis was performed by individuals blinded to both genotype and dietary treatment. For measuring cardiomyocyte cross-sectional areas from histology images, the micrographs were imaged and analyzed by an individual blinded to both genotype and diet intervention.
	Due to the complexity of study timing based on mouse age and assigning multiple small cohorts of mice to various treatment groups (discussed in 'Randomization' above), blinding was not performed during the termination of these studies (during animal sacrifices). Other than analyses described above, blinding was not performed for subsequent tissue analyses (namely gene and protein expression analyses) as these quantitative results were computer/software-generated based on all samples being treated in the same manner.

Reporting for specific materials, systems and methods

We require information from authors about some types of materials, experimental systems and methods used in many studies. Here, indicate whether each material, system or method listed is relevant to your study. If you are not sure if a list item applies to your research, read the appropriate section before selecting a response.

Materials & experimental systems

n/a	Involved in the study
☐	☒ Antibodies
☒	☐ Eukaryotic cell lines
☒	☐ Palaeontology and archaeology
☐	☒ Animals and other organisms
☐	☒ Human research participants
☒	☐ Clinical data
☒	☐ Dual use research of concern

Methods

n/a	Involved in the study
☒	☐ ChIP-seq
☒	☐ Flow cytometry
☒	☐ MRI-based neuroimaging

Antibodies

Antibodies used	1) Anti-MPC1 Ab for detecting human MPC1: Cell Signaling Rabbit monoclonal Ab (D2L91) catalog #14462. 2) Anti-MPC2 Ab for detecting human MPC2: Cell Signaling Technology Rabbit monoclonal Ab (D4I7G) catalog #46141. 3) Anti-MPC1 and MPC2 antibodies for detecting mouse MPC proteins were generated by Dr. Michael Wolfgang at Johns Hopkins. 4) Anti-VDAC1: Abcam mouse monoclonal (20B12AF2) cat# ab14734. 5) Anti-OX PHOS antibody cocktail: ThermoFisher Scientific catalog #45-8099. 6) Anti-alpha-Tubulin Ab: MilliporeSigma mouse monoclonal (B-5-1-2) cat#T5168. 7) Anti-VLCAD: rabbit polyclonal Ab was generated by Dr. Arnold Strauss at Washington University and was a gift of Dr. Strauss/ Dr. Daniel Kelly. 8) Anti-LCAD: rabbit polyclonal Ab was generated by Dr. Arnold Strauss at Washington University and was a gift of Dr. Strauss/ Dr. Dan Kelly. 9) Anti-MCAD: rabbit polyclonal Ab was generated by Drs. Dan Kelly and Arnold Strauss at Washington University and was a gift from both of them. 10) Anti-CPT1B (CPT1-m): Alpha Diagnostic International rabbit polyclonal cat#CPT1M11-A. 11) Anti-BDH1: ThermoFisher Scientific mouse monoclonal (1A5) cat#MA5-15594. 12) Anti-phospho ERK1/2 (phospho-p44/p42): Cell Signaling Technology rabbit polyclonal Ab cat#9101. 13) Anti-ERK1/2 (p44/p42): Cell Signaling Technology mouse monoclonal Ab cat#4696. 14) Anti-phosphoAMPKa (Thr172): Cell Signaling Technology rabbit monoclonal (40H9) Ab cat#5256. 15) AntiAMPKa: Cell Signaling Technology rabbit polyclonal cat#2532. 16) Anti-phospho-mTOR (Ser2448): Cell Signaling Technology rabbit monoclonal (D9C2) Ab cat#5536. 17) Anti-mTOR: Cell Signaling Technology rabbit monoclonal (7C10) Ab cat#2983. 18) Anti-phospho-S6 Ribosomal Protein (Ser 235/236): Cell Signaling Technology rabbit polyclonal Ab cat#2211. 19) Anti-S6 Ribosomal Protein: Cell Signaling Technology rabbit monoclonal (5G10) Ab cat#2217. 20) Anti-beta-Actin: MilliporeSigma mouse monoclonal (AC-74) Ab cat#A2228. 21) Anti-Rabbit IRDye Secondary Antibody: LiCor donkey 680RD (red; cat#926-68073). 22) Anti-Rabbit IRDye Secondary Antibody: LiCor donkey 800CW (green; cat#926-32213). 23) Anti-Mouse IRDye Secondary Antibody: LiCor donkey 680RD (red; cat#926-68072). 24) Anti-Mouse IRDYE Secondary Antibody: LiCor donkey 800CW (green; cat#926-32212).
Validation	1) The Anti-MPC1 Ab for detecting human MPC1 was validated by western blotting and probing for human expression constructs and visualizing increased MW with corresponding protein tags. https://www.cellsignal.com/products/primary-antibodies/mpc1-d2l9i-rabbit-mab/14462?site-search-type=Products 2) The Anti-MPC2 Ab for detecting MPC2 has been validated by western blotting for CRISPR-knockout cells as well as human cell lines with mutations in MPC1/MPC2 that disrupt expression https://insight.jci.org/articles/view/126132 3) The anti-MPC1 and MPC2 antibodies for detecting mouse MPC proteins have been validated by previous studies in knockout and hypomorphic mice (https://www.sciencedirect.com/science/article/pii/S1550413115003915?via%3Dihub; https://www.sciencedirect.com/science/article/pii/S2211124714003921?via%3Dihub; https://mcb.asm.org/content/36/15/2089.long) 4) The anti VDAC1 Ab was validated in WT and KO human human cell lines as described in product literature (https://www.abcam.com/vdac1-porin-antibody-20b12af2-ab14734.html#description_images_1) 5) The Anti-OX PHOS antibody cocktail is used for the detection of electron transport system subunits in complexes I-V according to manufacturers directions (https://www.thermofisher.com/antibody/product/OxPhos-Rodent-WB-Antibody-clone-Cocktail-Cocktail/45-8099). The antibody has been used extensively in previous publications for this purpose (https://www.nature.com/articles/s41598-017-16077-y; https://febs.onlinelibrary.wiley.com/doi/full/10.1002/1873-3468.12549; https://www.nature.com/articles/ncomms5993) 6) The Anti-aTubulin ab was used according to manufacturer's directions to detect aTubulin as a loading control. Antibody has been used previously for this purpose in numerous animal tissue/cell types (TOGp, the human homolog of XMAP215/Dis1, is required for centrosome integrity, spindle pole organization, and bipolar spindle assembly. Cassimeris L and Morabito J Molecular Biology of the Cell 15(4), 1580-1590, (2004); Increased expression of αTubulin is associated with poor prognosis in patients with pancreatic cancer after surgical resection Lin C, et al. Oncotarget 7(37), 60657-60657, (2016); https://www.nature.com/articles/s41467-019-11671-2) 7) The Anti-VLCAD Ab was generated by Dr. Arnold Strauss and validated by western blotting for WT, Heterozygous, and KO mouse heart tissue (https://www.ahajournals.org/doi/pdf/10.1161/01.RES.0000088786.19197.E4) 8) The Anti-LCAD Ab was used to detect LCAD in heart tissue in a similar manner as reported previously (https://www.sciencedirect.com/science/article/pii/0167478193900156) 9) The Anti-MCAD Ab was generated and used previously to detect MCAD by western blotting in both tissue lysates and with purified protein (https://www.ncbi.nlm.nih.gov/pmc/articles/PMC305023/pdf/pnas00277-0125.pdf) 10) The Anti-CPT1B antibody was used according to manufacturer's recommendations (https://www.4adi.com/product/pdf/CPT1M11-S-A-P.pdf) and has been used previously to detect CPT1B in mouse tissues (Cheng L, 2004, Nature Medicine 10, 1245 – 1250; Britton CH et al (1997) Genomics 40, 209-211) 11) The Anti-BDH1 Ab was used according to manufacturer's directions and has been used previously in mouse hearts, with validation by increased BDH1 expression in a mouse line of a transgenic mouse line of E2F which increases BDH1 expression (https://journals.plos.org/plosone/article?id=10.1371/journal.pone.0170066) 12) The Anti-phospho-ERK1/2 Ab was used according to manufacturer's instruction and has been used extensively to study ERK phosphorylation at Thr202 and/or Tyr204 (https://www.cellsignal.com/products/primary-antibodies/phospho-p44-42-mapk-erk1-2-thr202-tyr204-antibody/9101) 13) The Anti-ERK Ab was used according to manufacturer's instruction and has been used extensively to study ERK (https://www.cellsignal.com/products/primary-antibodies/p44-42-mapk-erk1-2-l34f12-mouse-mab/4696) 14) Anti-phosphoAMPKa Ab was used according to manufacturer's suggestion and is validated by increased expression of cells treated by H2O2 and decreased expression in cells in the absence of a phosphatase (https://www.cellsignal.com/products/antibody-conjugates/phospho-ampka-thr172-40h9-rabbit-mab-biotinylated/5256) 15) AntiAMPKa Ab was previously validated by western blotting for AMPKa -/- MEF cells (https://www.ncbi.nlm.nih.gov/pmc/articles/PMC1592699/) 16) Anti-phospho-mTOR (Ser2448) Ab was used according to manufacturer's suggestions and was validated by western blotting in cells treated +/- insulin (https://www.cellsignal.com/products/primary-antibodies/phospho-mtor-ser2448-d9c2-xp-rabbit-mab/5536)

17) The Anti-mTOR Ab was used according to manufacturer's suggestions and was previously validated by siRNA knockdown experiments (https://www.cellsignal.com/products/primary-antibodies/mtor-7c10-rabbit-mab/2983)

18) The Anti-phospho-S6 Ribosomal Protein Ab was used according to manufacturer's directions and was validated by western blotting for cells that were either serum-starved or treated with 20% FBS (https://www.cellsignal.com/products/primary-antibodies/phospho-s6-ribosomal-protein-ser235-236-antibody/2211)

19) Anti-S6 Ribosomal Protein was used according to manufacturer's instructions for detection of S6RP by western blotting in mouse cells/tissues (https://www.cellsignal.com/products/primary-antibodies/s6-ribosomal-protein-5g10-rabbit-mab/2217)

20) Anti-beta-Actin Ab was used according to manufacturer's instructions to serve as protein loading control in a variety of species tissue/cell types, including mouse (https://www.sigmaaldrich.com/catalog/product/sigma/a2228?lang=en&region=US)

21-24) IRDye Secondary antibodies used per manufacturer's instructions to detect mouse- or rabbit-generated primary antibodies (LiCor).

Animals and other organisms

Policy information about studies involving animals; ARRIVE guidelines recommended for reporting animal research

Laboratory animals	All mice were C57BL/6J both male and female and used between ages 6-19 weeks.
Wild animals	N/A
Field-collected samples	N/A
Ethics oversight	The Institutional Animal Care and Use Committees at Washington University and Saint Louis University approved the animal procedures for these studies.

Note that full information on the approval of the study protocol must also be provided in the manuscript.

Human research participants

Policy information about studies involving human research participants

Population characteristics	Heart tissue was collected from human subjects regardless of age, sex, genetics/genotypes. For subjects with heart failure, after consent, small sections of LV tissue were taken either at the time of left-ventricular assist device (LVAD) implant, or after heart transplantation. Failing Post-LVAD samples were taken after cardiac transplantation. Non-failing control heart tissue was obtained from diagnosed brain-dead individuals after organ procurement organizations determined unsuitability for use as donor hearts. The reasons these hearts were unsuitable for transplant varied, and was typically related to: advanced age, drug use, or excessive coronary artery disease (but not including heart failure).
Recruitment	Heart failure subjects were recruited at the cardiac care unit near the time of LVAD placement or heart transplant. Non-failing control hearts were not recruited, but were obtained from brain-dead individuals that provided organs for potential use in transplantation. There was no difference in willingness to participate (give consent for tissue collection) whether heart tissue was obtained pre- or post-LVAD implant (Failing vs Post-LVAD groups). This was likely due to the tissue needing to be removed during LVAD implant regardless of study participation. Thus, in both cases no excess tissue removal or excess risk was required in order to participate. The non-failing heart samples could not contain self-selection bias as they were obtained from brain-dead individuals willing to donate their organs.
Ethics oversight	Washington University IRB approved a protocol for the collection of heart tissue for this study.

Note that full information on the approval of the study protocol must also be provided in the manuscript.